PREDICTING THE DEFORMATION OF 3D PRINTED ABS PLASTIC USING MACHINE LEARNING REGRESSIONS

by

Justin Stellmar

Submitted in Partial Fulfillment of the Requirements

for the Degree of

Master of Science in Engineering

in the

Mechanical Engineering

Program

YOUNGSTOWN STATE UNIVERSITY

May 2020

PREDICTING THE DEFORMATION OF 3D PRINTED ABS PLASTIC USING MACHINE LEARNING REGRESSIONS

Justin Stellmar

I hereby release this thesis to the public. I understand that this thesis will be made available from the OhioLINK ETD Center and the Maag Library Circulation Desk for public access. I also authorize the University or other individuals to make copies of this thesis as needed for scholarly research.

Signature:

_____

Justin Stellmar, Student Date

Approvals:

_____

Dr. Darrell Wallace, Thesis Advisor Date

_____

Dr. Jason Walker, Committee Member Date

_____

Dr. Virgil Solomon, Committee Member Date

_____

Dr. Salvatore A. Sanders, Dean of Graduate Studies Date

ABSTRACT

FDM printing is a relatively cheap and fast method to produce parts as compared to traditional machining, which makes it attractive for many applications including tooling. Contrary to the isotropic behavior of steel tooling, the anisotropic properties of the printed materials can be attributed to FDM printing parameters. It is possible that through a proper machine learning regression model, the behavior of these parts could be captured, modeled and predicted. Predicting the deformation and stress of FDM created tools and dies could be an excellent way to save on costs for low run manufacturing due to its lower lead time, and manufacturing cost. FDM material behavior is complex and unpredictable by current testing standards, so as an alternative strategy, machine learning is proposed to model deformation and stresses. ABS cylinders were printed and compressed to depths ranging from .025-.150 inches. Fujifilm Prescale paper was used during compression to record the pressure distribution across the surface of the sample interface. The Prescale was scanned, converted to grayscale, and processed using MATLAB. Random points on the affected area of the pressure papers were selected exported. Data points were split into two bodies; one to create regression models and one to test the models. The first file was imported into MATLABS's regression learner to create regression models. Regression models were created with three different validation strategies and tested against holdout data to estimate predication accuracy. Residual model error for prediction of compression depth and stress distribution were compared. It was found that validation types had no impact on the RMSE of regression models for both the compression depth and grayscale value predictions. Compression depth for any of the samples could be predicted between 1 – 23 thousandths of an inch. Stress, which was represented as grayscale could be predicted within 293 thousandths of a grayscale. Grayscale is a unitless dimension which ranges from white (0) to black (1). Testing the model against samples used to build it led to an RMSE of 137 thousandths using a Bagged Trees regression. These numbers cannot be directly correlated to a range of stress due to a nonlinear relationship between grayscale values and stress, however the error is significant considering that the range of grayscale values measured ranged between 0.150 to 0.802. This method was excellent at predicting the deformation of samples that had dimensions used to create the regression models, and it was decent at predicting the deformation of samples that had at least one dimension not seen by the regression models. The method was poor at predicting grayscale values for any sample, regardless of whether it was seen by the model.

ACKNOWLEDGEMENTS

First and foremost, I wish to show my gratitude towards the MAMLS Grant as well as the Cushwa/Commercial Shearing Graduate Fellowship for funding me through my graduate studies. I would like to express my appreciation to my advisor, Dr. Wallace, for both suggesting and assisting me with this research topic. I would like to thank my committee members, Dr. Solomon and Dr. Walker, for providing me with valuable and constructive suggestions. I wish to show my gratitude towards everyone who provided me with feedback and assistance during my experimentation and writing processes including my graduate colleagues, the students from the CIAM lab, my mother, my two brothers, and Kim.

Lastly, I would like to thank my dog, Lucy, for keeping me company while I wrote.

TABLE OF CONTENTS

LIST OF FIGURES

LIST OF TABLES

NOMENCLATURE

P	pressure
E	error
x	variable
y	function of variable
$\hat{x}$,$\hat{y}$	estimation of parameter
β	real number coefficient
θ	unconstrained parameterization vector
σ_f	signal standard deviation
σ_l	signal characteristic length scale
R^2	coefficient of determination

Subscripts

0	reference point
f	final point

LIST OF ACRYNOYMS

ABS	Acrylonitrile Butadiene Styrene
AI	Artificial Intelligence
AM	Additive Manufacturing
AOI	Area of Interest
ASTM	American Society for Testing and Materials
ATOS GOM	Optical 3D Measuring Machine
BEM	Basic Ensemble Method
CAD	Computer Aided Design
CMYK	Cyan Magenta Yellow Black
CNC	Computer Numerical Control
CNN	Convolutional Neural Network
dpi	Dots per Square Inch
FDM	Fuse Deposition Modeling
FEA	Finite Element Analysis
GEM	General Ensemble Method
GLM	Generalized Linear Model
GP	Gaussian Process
LS	Laser Sintering
MATLAB	Matrix Laboratory
ML	Machine Learning
MS	Mono Sheet
PC	Polycarbonate
PET	Polyethylene Terephthalate
PLA	Polylactic Acid
RBF	Radial Basis Function
RMSE	Root Mean Square Error
RP	Rapid Prototyping
SAAM	Small Area Additive Manufacturing
SLA	Stereolithography
SLS	Selective Laser Sintering
STL	Standard Tessellation Language
SVM	Support Vector Machine
TIF	Tagged Image Format
TPU	Thermoplastic Polyurethane

CHAPTER 1

INTRODUCTION

In an industry that has been the centerpiece of American manufacturing, metal tooling and dies have given the ability to create consistent and precise metal formed components since the 19th century (Ulintz, 2015). When parts are mass produced, tooling costs diminish as more widgets are created. However, if only a small number of parts are needed, tooling costs can make creating a widget unjustifiable. With additive manufacturing (AM) and machine learning becoming more popular, the question arises if such technologies could be used for tooling and die creation. Fused Deposition Modeling (FDM) is a popular type of additive manufacturing that is commonly used in rapid prototyping (Prototype Projects, 2018). FDM printing is a relatively cheap and fast method to produce parts as compared to traditional machining. Contrary to the isotropic behavior of steel tooling, the anisotropic properties of the printed materials can be attributed to the parameter sensitive quality variability of the FDM process. It is possible that through a proper machine learning regression model, the behavior of these parts could be captured, modeled and predicted. Predicting the deformation and stress distribution of FDM created tools and dies could be an excellent way to save on costs for low run manufacturing due to its lower lead time, material cost, and manufacturing cost.

This thesis will explore whether machine learning regression modeling can be used to predict the deformation of FDM cylinders created under fixed parameters. This alternative modeling technique may play an important role in the future of the research and development by enabling the behaviors of 3D printed plastics to be predicted.

CHAPTER 2

BACKGROUND

2.1 Origin of 3D Printing

The term 3D printing has evolved from an earlier term for the process called rapid prototyping (RP). The intention of rapid prototyping was to have a more cost-effective method to prototype industry products. The first patent application for RP technology was submitted by a Japanese man in May of 1980 named Dr. Kodama (3D Printing Industry, 2017). Unfortunately, Dr. Kodama did not file the full patent specification before the required deadline and therefore never received a patent for his technology.

Soon after, 3D printing technologies began to originate, most of which are still commonly used today. In 1986, Charles Hull patented the first stereolithography apparatus (SLA) which uses an ultraviolet laser to turn a liquid resin into a solid (Cyant, 2017). Over the next decade many more additive manufacturing processes were developed including Selective Laser Sintering (SLS), Fuse Deposition Modeling (FDM), and Laser Sintering (LS). These technologies have come a long way since their first patent. The machines being used to additively manufacture parts have significantly improved in manufacturing quality and affordability. The first 3D SLA printer created by Charles Hull used to cost around $300,000 in 1987. However, thanks to crowdfunding campaigns such as Kickstarter as well as a high demand from consumers, a respectable 3D printer in 2016 could be purchased for $1800 or less (Miller, 2016).

2.2 3D Printing Process

There are seven main categories of additive manufacturing; Vat photopolymerization, material jetting, binder jetting, material extrusion, powder bed fusion, sheet lamination, and direct energy deposition (Loughborough University, n.d.). Although the materials and procedures used to create AM parts may vary, the printing preparation between these processes are more-or-less the same. To begin, the printing preparation process will be laid out.

2.2.1 Creating an Additively Manufactured Part

There are three main steps to preparing a 3D printed component (Engkvist, 2017):

1. Creating a part to be printed using a Computer Aided Design (CAD) program.
2. Tessellating the CAD geometry into a Stereolithography (STL) format. This step creates triangular representation of a 3D object (McCue, 2019) and allows the model to be converted into multiple surface meshes that differentiate the interior and exterior of the model.
3. Slicing the geometry into layers. With respect to the print orientation, layers are introduced to the geometry, and slice it in the z axis. Points of intersections between the layers and the surface mesh are recorded as nodes by the printing software. Like a connect the dot puzzle, the printer head moves from point to point on a predetermined path to build each layer.

Different printers are compatible with different slicing file types. A common output file type for slicing parts is G-code. G-code was originally created for Computer Numerical Control (CNC) machining. Within G-code, important information is stored and used by the machine such as tool paths and speeds (Star Rapid, 2016). Using G-code was intuitive for AM since the primary use of the code is for controlling the path and speed of tools.

2.2.2 Fuse Deposition Modeling

Fused Deposition Modeling (FDM) falls under the material extrusion category of additive manufacturing and was the process that was used for this research topic. Material extrusion is currently the most popular AM process when comparing consumer demand and quality (Engineering Product Design, n.d.) to other types. Samples printed for this project were done so by using a Lulzbot TAZ Pro 3D printer which uses the FDM process to produce parts.

The FDM process was invented in 1989 by Scott Crump who later became a co-founder of Stratasys (Gibson, Rosen, & Stucker, 2010). With Crump's form of FDM printing, the printer uses two different types of printing material (Palermo, 2013). Both materials are fed to the printer from spools of continuous filament into an extruding nozzle where the material is then heated and deposited onto the build area. The first material is referred to as modeling material. Modeling material constitutes the final printed piece. The second material is an alcohol soluble support

material. The support material is extruded simultaneously with the modeling material and creates a supportive body around the printed part.

Once the printed piece is complete, the object is soaked in a detergent based solution where the support material dissolves into the solution. The finished model is usually of good surface quality but can be further post processed through sanding, bead blasting, or vapor smoothing (Frick, 2014).

Alternatively, parts can be created with a support structure rather than support material. Support structures closely resembles scaffolding and are used to reduce deformations of overhanging regions on the part. Since only one material is used in the printing, this method is usually more cost effective. The downside to this alternative is the surface bumps that remain after the support is removed. Support material can be removed by cutting or breaking the support from the part. Further post processing to smooth the outer surface can be done through sanding, and in the case of ABS plastic, vapor smoothing the outer surface by placing the part in an acetone vapor environment.

2.2.3 FDM Materials

The popularity of FDM printing has produced a plethora of printable materials. Historically, Polylactic Acid (PLA) and Acrylonitrile Butadiene Styrene (ABS) have been the most common polymers used (3D Matter, n.d.). More recently other polymers have been used such as Polyethylene Terephthalate (PET), Nylon, Thermoplastic Polyurethane (TPU), Polycarbonate (PC).

Some materials require different nozzle materials to resist erosion due to material passing through the print head. The three common nozzle materials for FDM printing are made of brass, stainless steel, and hardened steel. Non-abrasive/non-reinforced materials such as PLA or ABS use brass. More abrasive materials, such as Carbon filled Nylon or Glass filled Nylon require hardened steel to prevent rapid nozzle erosion (3DXTECH, 2020).

2.3 3D Printing Uses in Industry, Research & Development

3D Printing technology has slowly been making its way into practical applications in the real world. Applications are currently being introduced to, but are not limited to, the dental, surgical, aerospace, and metal forming industries. Examples of the

uses and impacts that 3D printing has had on these industries are outlined in the following sub-categories.

2.3.1 Dental

The dental industry has arguably adopted 3D printing technology faster than any other industry. Oral scanners are being combined with FDM printers to create teeth aligners. Stratasys performed a user case study on an orthodontics company called DynaFlex. Located in St. Ann, Missouri, DynaFlex specializes in printing aligner arches. Aligner arches are used as a mold to create clear aligners for straightening teeth. Clear aligners are a less invasive alternative to braces. The ability to rapidly produce the arches grants DynaFlex the ability to greatly increase their potential output without sacrificing quality (Buddemeyer, 2018). Although their previous production capacity was unstated, DynaFlex can print up to 1,500 arches per day in house.

Outside of plastic printing, the dental industry is now using wax printers to create molds for lost wax casting patterns (Prod Ways Tech, n.d.). The lost wax casting process involves creating an object that is to be casted in metal out of wax, printing the object in wax, coating the wax object in a ceramic slurry to create a mold, melting the wax out of the mold, and pouring the desired metal into the mold (3DSourced, 2018). This process is being used in the dental industry to create objects such as removable partial dentures, bridges, and crowns. The high precision and good burn-out properties of the 3D printed wax make this process a cost and time effective solution for dentists. Other dentistry companies such as Align Technology, the makers of Invisalign, have taken on SLA printing technology to create invisible aligners to teeth straightening. As of 2018 Align Technology, along with the help of 3D Systems ProX SLA 3D printer, were able to create over 1.6 million patient-ready aligners per week (Griffiths, 2018).

2.3.2 Aerospace

An aerostructure and engine system company, GKN Aerospace, has implemented FDM 3D printing to create tools as well as jigs and fixtures. They have begun productions using the Stratasys F900 FDM machine to produce components with ULTEM 1010. The purpose of their implementation was to create parts rapidly that could not otherwise be created with traditional manufacturing methods (Davies, 2018). When interviewed by the press, the Additive Manufacturing Center Manager, Tim Hope stated:

> "We can now cost-effectively produce tools for our operators within three hours. This saves critical production time, and by printing in engineering-grade thermoplastic, we can produce 3D printed tools with repeatable, predictable quality every time. All the while matching the quality of a traditionally-produced tools, and reducing the costs and concessions compared to equivalent metallic tooling."

Metal printing is also being introduced to the aerospace world. Topology optimization is being performed on bulky parts to reduce the weight of the plane, and large companies such as GE, Boeing, and Airbus are developing functional prototypes of turbine components (3D Natives, 2018). With the aerospace industry being as highly-regulated as it is, companies like Materialise are focusing on determine the strength and functional requirements of 3D printed components that would allow them to be used on normal aircraft (Crutchfield, 2018). Materialise focuses on AM process control to achieve repeatable prints of almost any AM material available to consumers.

2.3.3 Metal Forming

In the metal forming industry, some small-scale manufacturers have used the FDM process to create plastic tooling for brake presses. First was Rainbow Aviation, who documented their use of Z-Ultrat to create dies for a press brake. The tooling was used in a 20-ton CNC hydraulic press to bend light gauge 2024-T3 aluminum for use in an airplane. Tools were printed on a Zortrax M200 at 100% infill (Rainbow Aviation Services, 2018) and consisted of both a male and female side. Approximately 30 metal components were formed with satisfactory quality. No precise measurements were taken to check for tooling wear; however, the proof of concept was successful, and the parts were able to be used.

A somewhat better documented study of 3D printed tooling for metal forming was performed by Cincinnati Incorporated. From their testing they concluded that tooling made from PLA has a niche in the manufacturing world for creating short-run, proof of concept, and peripheral assembly items (Coleman, 2019) due to its low cost and lead time, and its looser tolerances when compared to traditional metal tooling. None of the plastic tooling tested broke when it was used to form mild steel up to 12 gauge. It was estimated that a tool built in a Small Area Additive Manufacturing (SAAM) printer could perform about 1,000 hits before needing replaced.

Stretch forming is a process that involves forming a sheet of metal by stretching and bending it simultaneously over a contoured die. With stretch forming commonly being used for low production parts, the Advanced Metal Forming Group at Ulster University studied the idea of stretch forming parts using a 3D printed die. For the testing, 3mm thick 5083 aluminum was used as the metal to be formed. The 3D printed tool was created using the FDM process and PLA material. A 15% infill of a square grid was used internally, and a 5mm wall thickness was used across the part. Although wear was not assessed during the experiment, the part was able to be formed over the AM die with only very minor damage to the die at the points were pressure due to contact stress was highest (Leacock, Volk, McCracken, & Brown, 2017).

A study was performed on repeatability of sheet metal stamping tailgate reinforcement brackets. Two different sheets of metal, DC04 and S355 MC, were formed using polycarbonate dies printed on a Fortus FDM machine. 100 parts were created with both materials. Every ten parts, the dies were inspected with ATOS GOM optical scanning technology to measure geometric deviations across the printed parts. The results of the study concluded that DCO4 deviation of the die deviated within manufacturing tolerances, however S355 MC parts deviated higher than allowable. The conclusion was that the tailgate reinforcement brackets could be manufactured using the DCO4 material for low run productions. Geometric deviation was attributed to spring back and plastic deformation of the printed dies (Durgun, 2015).

2.4 Material Property Testing for ABS

With some materials, mechanical properties can vary depending on the orientation that the material is tested in. When a material exhibits the same mechanical properties in all directions, that material can be referred to as isotropic. In the case that the material behaves differently in various directions, that material is referred to as being anisotropic or aeolotropic (Gere & Goodno, 2012). Additively manufactured ABS plastic, along with others, behave anisotropically. This section discusses different ways that researchers have tried to capture the material behavior of these materials.

2.4.1 Testing of Traditional ABS

Polymers such as ABS predate AM methods. The most common testing methods used for testing these plastics were developed by the American Society for Testing

and Materials (ASTM). Under the ASTM D4673 testing standard, a list of testing procedures can be found for testing different grades of injection molded or extruded ABS plastic including recycled ABS but does not cover compression molding. Following this procedure will enable the tensile strength at yield, modulus, Charpy impact, vicat softening point, heat deflection temperature, and glass content of glass-reinforced materials (ASTM D4673-16, 2016).

2.4.2 Testing of FDM ABS

Testing of ABS is difficult, and is still a work in progress, hence this thesis. There have been many attempts at creating a reliable process to measure the material properties of 3D printed ABS plastic and predict its behavior. This section will discuss some of the proposed methods for achieving this.

A study was performed by students from the University of Florida, Bartram Trail High School, and The University of California at Berkeley to measure the material properties and the extent of anisotropy in 3D printed ABS and Polycarbonate parts. The sample set included parts printed at varying raster angles and build orientations to determine the directional properties of the materials. Tensile dogbone and shear Isopescu samples were built and 2D digital image correlation was used to measure strain (Cantrell, et al., 2016). A schematic of the contour of these samples can be found in Figure 2.1. The testing procedures followed ASTM standards D-638 for tensile specimens and D-5379 for shear specimens. The standards used were created to test general plastics and composite materials respectively. The findings from this study claimed that raster and build orientation had a negligible effect on the modulus of elasticity and Poisson ratio for ABS and that shear modulus and shear yield varied by up to 33%. This demonstrated that there was no correlation between tensile and shear properties.

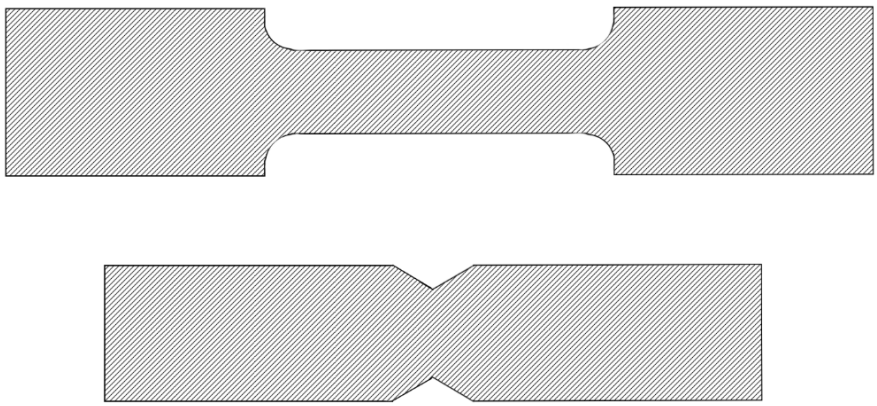

Figure 2.1: Dogbone Sample (Top) and Isopescu Sample (Bottom)

Another test was performed by a collaboration between Bucknell University and Duke University to measure the material properties of ABS printed using the FDM process. ASTM standards D3039 and D3479 were used to test the tensile properties and tensile fatigue of the material respectively. These standards were created to test polymer matrix composite materials which arguably describe FDM parts more accurately than general plastics or composite materials. The conclusion of this test stated that the anisotropic behavior of the ABS specimens was significantly influenced by the orientation of the layered rasters which created the directionality of the polymer molecules as a result. Other influences such as the presence of air gaps and the air void quantity between the rasters effected the strength and effective moduli in all tests completed (Ziemian, Sharma, & Ziemian, 2012).

The two studies discussed above had different opinions on the effect that the raster pattern had on the material properties. One study claims that raster and build orientation are negligible and test results can vary widely; the other claims that raster and build orientation are significant and test results are consistent to the parameters. Though most tests published in scientific literature used similar procedures, the results varied independently. This illustrates the difficulty of developing a suitable model to test 3D printed plastics.

A third study, performed by (Zou, 2016) studied the material properties of ABS printed on a Dimension SST 1200es made by Stratasys. Dogbone shaped samples were printed at a fixed bed temperature, nozzle temperature, and layer heights. However, the dogbone samples were printed at different angles including 0, 30, 45, 60, and 90 degrees. In the tensile testing machine both biaxial and uniaxial stain gages were attached to the samples. Both an isotropic and anisotropic model were

able to be obtained. This study was able to find a relationship between tensile and shear modulus for each orientation.

2.5 Machine Learning

Due to the variation of FDM material test results published, one could wonder if there is a better way to determine the material properties of a 3D printed part. With Machine Learning (ML) becoming more common among computational software packages there may be a way to integrate ML into 3D printing and ultimately better understand the material behavior of 3D printed part.

2.5.1 What is Machine Learning?

The concept of machine learning is not new; in fact, the term *machine learning* was first used by Arthur Samuel in 1959 (Samuel, 1959). Machine learning is the study of algorithms and statistical models that a computer uses to perform tasks without explicit instructions. Rather than relying on user input for instructions, the computer uses patterns and inference instead (Koza, Bennett, Andre, & Keane, 1996).

2.5.2 How Machine Learning Works

Machine learning is seen as a subset of Artificial Intelligence (AI). It enables a computer to build and train a mathematical model based on input commonly referred to as training data. Once a trained model is complete, the model can process new inputs and make predictions or decisions based upon its previous knowledge alone (Bishop, 2006).

Machine learning uses two different types of techniques: supervised learning and unsupervised learning. In supervised learning the target concept is determined through class affiliation. In unsupervised learning the target concept is determined through intrinsic structures of the data (Zhao & Liu, 2007).

The concept of supervised learning is essentially feeding input-output pairs to a program which are mapped to create a function. The function can take a given input and predict an output. Supervised learning is learning when the inputs and outputs are known (Russell & Norvig, 2010).

Contrary to supervised learning, unsupervised learning is a type of self-organized learning in which patterns are formed from a data set without the help of input or output labels (Hinton & Sejnowski, 1999). This means that the unsupervised learner is capable of learning relationships using supervised learner methods, in other words, it can predict future percepts using previous percepts (Russell & Norvig, 2010).

Within the supervised and unsupervised learning techniques there are different methods to manage the information of interest. Some of the most popular unsupervised learning methods are principal component and cluster analysis. Additionally, popular supervised learning methods are called classification and regression. The relationships between machine learning, learning techniques, and the technique methods can be better visualized using Figure 2.2. These ML methods will be further discussed in the following sections.

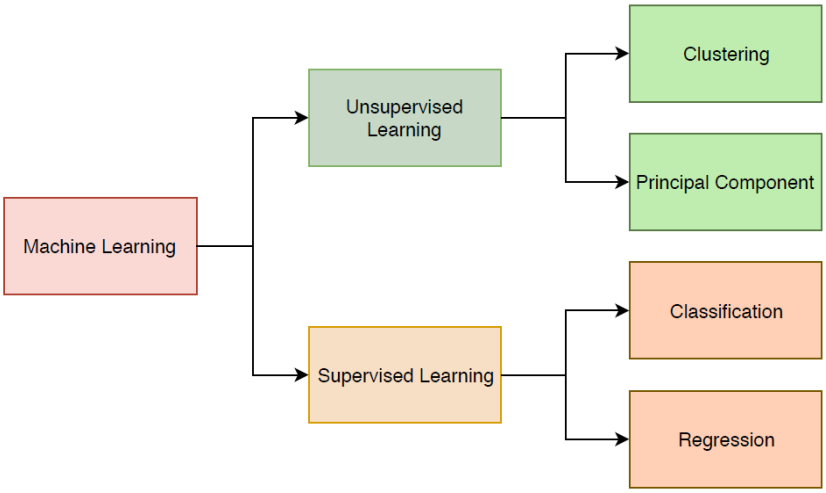

Figure 2.2: Machine Learning Methods Visualized

2.5.3 Unsupervised Learning Methods

The principle component analysis is mainly used in exploratory data analysis where the main characteristics of data are summarized and usually represented as visual outputs. The intent was to make data analysis more precise, accurate, and easier for statisticians in addition to finding outliers worth researching further (Tukey, 1961). The principle component method only has one algorithm in itself.

Rather than generalizing the group, the cluster analysis is used to divide a body of data into groups or clusters, however the cluster analysis includes a very large

number of algorithms to complete the task. A cluster algorithm designed for one type of data set model will likely fail when used on another (Estivill-Castro, 2002).

2.5.4 Supervised Learning Methods

Classification is the process of determining which set of categories a new observation belongs. This principle can apply to concepts such as email where a program needs to determine if a new email is spam or normal mail. Popular classification techniques are support vector machines, discriminant analysis, naïve Bayes, and nearest neighbor. The benefit of classification techniques, especially in data mining, is the ability to process and categorize large amounts of data based off a training set and class labels (Nikam, 2015).

Regression is a data mining function that predicts a number by fitting an equation to a data set (Dokania & Navneet, 2018). However, the regression technique is broader than a basic linear regression algorithm. Regression learning can also use the generalized linear model (GLM), Support Vector Machines (SVM), Gaussian Process (GP), Ensemble Methods, and Decision Trees.

For a better understanding on how machine learning types, models, and model types work together refer to Figure 2.3 below.

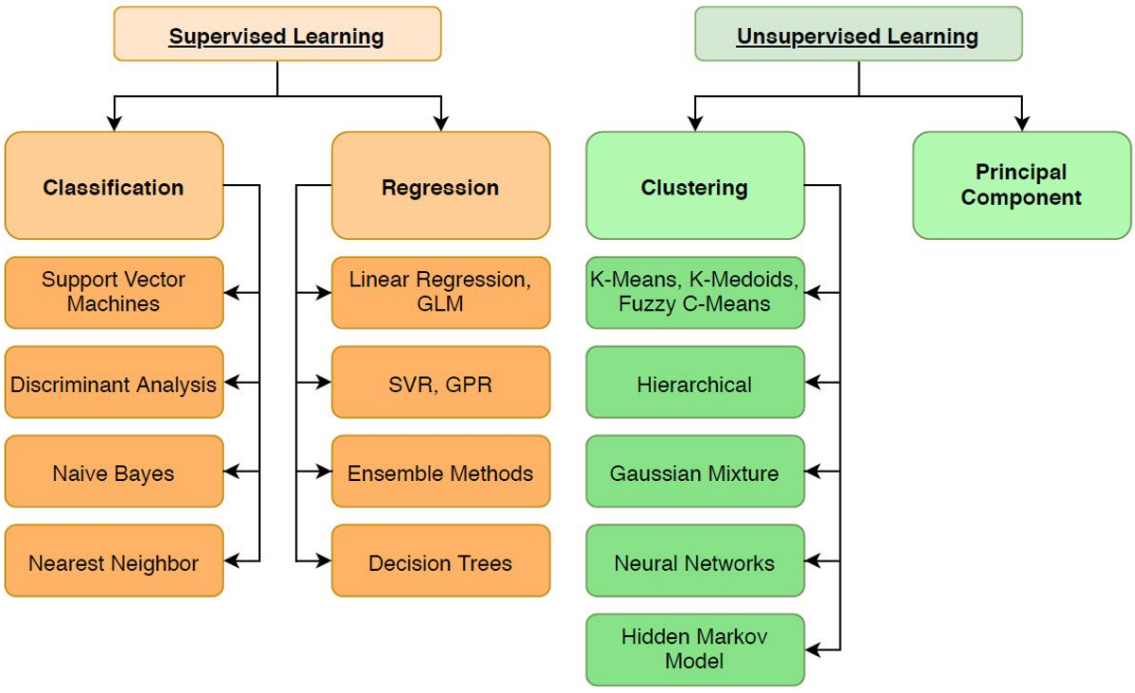

Figure 2.3: Machine Learning Algorithm Relationships

2.5.5 Regression: Linear Models

A regression is a model that can determine a value based on independent predictors. Linear regressions are performed by finding a best fit line that matches the slope of the independent predictors. The output of a linear regression will always be a value that falls somewhere on the best fit line (Gandhi, 2018). Results made by ML linear regression models are easy to interpret but have low predictive accuracy due to their highly constrained form (The MathWorks, Inc., 2019). A linear regression model generally exists in the form of Equation 2-1 below where y is the predicted output, x is the independent input, and β is a coefficient. The "hat" notation over the letters indicates an estimate of a parameter. Parameters are unknown quantities that characterize a model whereas estimates of parameters come from computable functions of data, making them a statistic (Weisberg, 2005).

$$\widehat{y_i} = \beta_0 + \beta_1 * \widehat{x_i} \qquad 2\text{-}1$$

2.5.6 Regression: Support Vector Machine

Support vector machines work by plotting input data as a point in an n-dimensional space with the value of the point being its coordinate. With all data points plotted, the values are separated with a hyper-plane. A hyper-plane is a plane/line that separates the data points into two separate groups of information. Support vectors are used to define the margin of largest separation between the two groups (Cortes & Vapnik, 1995). Figure 2.4 below shows an example of a simple SVM application in a 2-dimensional space. The data points are separated into two groups, as shown by the red diamonds and purple circles, by the hyper-plane between them. For this case, a hyper-plane would work anywhere within the optimal margin, however best results will come by creating an optimal hyper-plane.

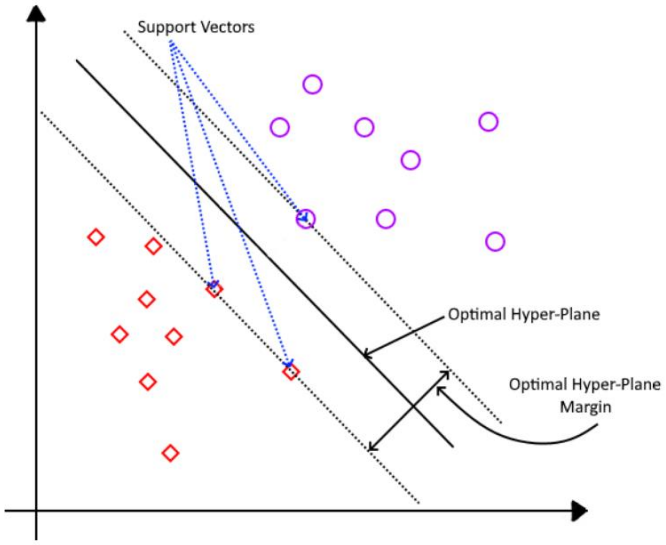

Figure 2.4: Simple Plot for SVM Explanation

By maximizing the margin between a data point and a hyper-plane, an optimal hyper-plane can be created. Optimal hyper-planes are determined using support vectors. Support vectors are a small subset of the training data. The decision function of an SVM is fully determined by the support vectors (Wang, Neskovic, & Cooper, 2005). A large amount of support vectors usually indicates non-separable data. If the training vectors can be separated without errors by a hyper-plane, the expected probability of an error committed on a test is bounded by the ratio between the expectation value of the amount of support vectors and the amount of training vectors (Vapnik, 1982). The relationship is show in equation 2-2.

$$E[\Pr(error)] \leq \frac{E[support\ vector\ count]}{training\ vector\ count} \qquad 2\text{-}2$$

Although the model shown had a clear distinction between the two groups of data points, in practical applications this is not usually the case. If a small number of outliers from one data set exist in another, they will usually be ignored for the analysis. If the data points are more intertwined, the option of using a kernel function is available. A kernel function will determine the non-linear transformation that is performed on that data prior to training the SVM (The MathWorks, Inc., 2019). Types of kernel functions used are the Radial Basis Function (RBF), linear kernel, quadratic kernel, and the cubic kernel. When processing data, the SVM works well for data sets that are small but have a high number of dimensions (Ray, 2017).

2.5.7 Regression: Gaussian Process

A Gaussian process is defined as the collection of random variables, any finite number of which have a joint Gaussian distribution (Rasmussen & Williams, 2006). With traditional non-linear regressions, a nonlinear curve is fit to a set of data points. Usually as the order of the polynomial is increased, so is the fit to the data set. However, in the case where more data points are introduced, it may be observed that a different function may fit the data set better. This is where the Gaussian Process comes into play.

To begin a Gaussian Process, a covariance function is necessary to define the relationships between the random input variables. Covariance is a functions property to retain its form when the variables are linearly transformed. It is likely that some points with similar predictor values x_i will have a close response value y_i (Rasmussen & Williams, 2006). The covariance function expresses the covariance between two latent variables designated as $f(x_i)$ and $f(x_j)$. A covariance function can be defined by multiple kernel functions. For standard kernel functions such as the Squared Exponential Kernel or the Exponential Kernel, the parameters behind these functions are based on the signal standard deviation and characteristic length scale which can be represented by σ_f and σ_l respectively. There exists a value at which the input value and response value can become uncorrelated. This value is defined as the characteristic length. For a kernel to function, the values of σ_f and σ_l both need to remain above zero. To ensure this is the case, an unconstrained parameterization vector θ is used (The MathWorks, Inc., 2019). The relationship of the unconstrained parameterization vector can be reviewed below in equations 2-3 and 2-4.

$$\theta_1 = \log \sigma_l \qquad 2\text{-}3$$

$$\theta_2 = \log \sigma_f \qquad 2\text{-}4$$

Once the covariance matrix is created, the Gaussian Process can be implemented on the data. For example, assume a 6-dimensional problem is to be analyzed with a specified number of data points. For any data point, the six variables can be plotted with one another to create a line that could be fitted by a non-linear regression. As each data point is iterated, a range of possible values for the six points can be established. With an independent variable selected, the variable with the highest fluctuation would be considered the least correlating to the independent variable while the variable with the smallest fluctuation would be considered the highest

correlation. Ultimately a family of curves is created that represents the variation of each variable. To better visualize this range, Figure 2.5 below shows a plot. The blue circles indicate an estimated mean and the blue lines intersecting the circles vertically indicate an estimated range of uncertainty. This graph is a visualization of the family of curves referred to earlier. Using these randomly generated curves, the mean and variance of the fitting can be computed (Turner, 2016).

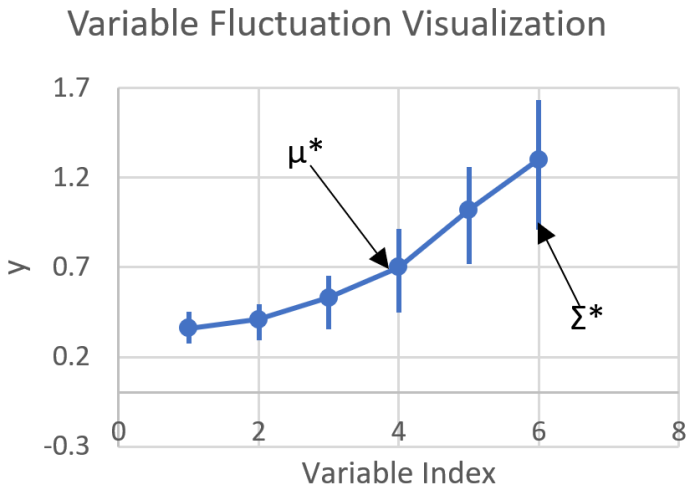

Figure 2.5: Variable Fluctuation Visualization

2.5.8 Regression: Ensemble Methods

Basic ensemble methods, also referred to as statistical resampling techniques such as jackknifing, bootstrapping, and cross validation use bias reduction to produce improved regression estimates (Perrone & Cooper, 1992). These techniques use resampling to improve an estimate of a given statistic, x. A final estimate can be reached through subsampling or resampling a finite data set, and combining the multiple estimates of x.

The jackknife method works by removing any single data point from a data set and developing an estimate of x using the remainder of the data set. The estimate is then tested on the removed data point, and this process is repeated for all data points in the data set. This process can be expedited by removing subsets from the data points.

Bootstrap aggregating, also known as Bagging, working by creating new data sets by randomly sampling and replacing points within the original data set. The newly created data sets are then used to create multiple estimates of x. This method, as

well as the jackknife method described above, take a large amount of computational power with respect the methods described below.

More advanced ensemble methods work by constructing a set of classifiers and using those classifiers to categorize new data points. The classification of new data points is performed by taking a weighted vote of the classifier's predictions (Dietterich, 2000). For an ensemble of classifiers to be more accurate than any of its individual members, the classifiers need to be both accurate and diverse (Hansen & Salamon, 1990). In the case of a Basic Ensemble Method (BEM) regression analysis, the classifiers are functions which are created by population of regression estimates through averaging in functional space (Perrone & Cooper, 1992). However, the BEM hold two assumptions. First, the base models are independent and second, the error of each base model holds a mean of zero. This method does not always hold up well for practical applications of ensemble methods, so the Generalized Ensemble Method (GEM) is typically used. Contrary to the BEM, the GEM discards base models that are correlated too closely. A close correlation is measured by the similarity of the predictions (Reid, 2007).

Lastly, the cross validation method which can be used as an ensemble method or for validating other models. Cross validation works by splitting a data set into K divisions with $K \leq$ data points. One partition of the data is referred to as the training data which is used to estimate a value of x, and the other partition is referred to as testing data, which is used to measure the accuracy of the estimate (Krogh & Vedelsby, 1994).

Cross validation is very useful in training networks to avoid overfitting. There are two main categories of cross validation: exhaustive and non-exhaustive. Exhaustive cross validation types divide the original data set and test it in all possible ways. Examples of exhaustive types are Leave-p-out, Leave-One-In, and holdout. Non-exhaustive cross validation types do not compute all possible ways of splitting the data set. A popular type of non-exhaustive cross validation is k-fold.

2.5.9 Regression: Decision Trees

Decision trees can be used for both regression and classification. All trees begin at the root node and work their way down to the leaf nodes. In regression, leaf nodes hold numeric responses. The input value is compared to the leaf responses so that a decision can be reached (The MathWorks, Inc., 2019). Decision trees are simple to interpret and more useful in classification applications.

2.5.10 Machine Learning Software

Machine learning software is a new software product that is being offered by a wide range of companies. Larger companies such as Google and IBM are offering both model training and predictive modeling, however, their software packages lack statistical or mathematical functions. Other options such as Python can run open source ML software such as H20 and SciPy.

It was preferential to use a program that had ML software built in and offered professional support. For this experiment, the program MATLAB was used. Within MATLAB is an add on called the statistics and machine learning toolbox which offers all regression methods of interest.

2.6 3D Printing and Machine Learning

Machine learning has been finding its way into the additive manufacturing industry in various ways. A large portion of research combining the two topics exists in AM metals rather than plastics. One research topic includes using a thermo-mechanical Finite Element Analysis (FEA) software to simulate shrinkage and deformation of an AM part, the deformed surface coordinates from the FEA are extracted and used as inputs for the ML model. The ML model is used to make geometric corrections to the parts which in turn are implemented to an STL file for printing. The modified part results in an accurately dimensioned finished product (Chowdhury & Anand, 2016). Another research topic involves real time in situ quality control during printing. In situ is synonymous with the phrase “in the original place”. The process works by using a vision system composed of high-speed cameras used for process image acquisition. The cameras can detect melt pool, plume, and splatter as it occurs. Two classification methods were studied: support vector machines and Convolutional Neural Network (CNN). With the SVM method, features of the objects created are extracted and fed into an ML algorithm. The results of this method showed that information from different objects is sensitive to different types of quality anomalies (Zhang, Hong, Ye, Zhu, & Fuh, 2018). These are just two of many potential applications for ML and metal printing integration.

Machine learning in the FDM realm of AM also comes with its share of integrations. For example, a study was performed by (Wu, Wang, & Yu, 2016) to perform in situ monitoring of the condition of an FDM machine using acoustic monitoring. Monitoring was focused on identifying machine breakdowns. The breakdowns include issues such as nozzle blockages. Support vector machines were used to

classify different time and frequency domains that were associated with breakdowns. The goal of this technology implementation is to create a closed loop feedback program that will tell the machine when an error occurs to help prevent machine damage. Another study was done on the material properties of FDM objects. Rectangular prisms were made, and process parameters such as layer height, orientation, and raster angle were varied using the same geometry. Compressive strength was taken of all of the samples, and the printing parameters and compression strength of the different samples were used as inputs for a ML regression algorithm in order to determine how different parameters affected the compressive strength of a part (Panda, Bahubalendruni, & Biswal, 2015).

CHAPTER 3

EXPERIMENTAL DESIGN

This chapter will outline the experimental design. Once a tooling material is selected, samples will be created for compressive testing. All samples were cylindrical, having various cross sections and heights. By compressing the plastic tooling between hard steel surfaces and a sheet of FujiFilm Prescale, the pressure profile between the contact surface of a 3D printed material and the steel plate can be obtained. First, a set of samples are compressed through a range of depths to determine which depth develops the film best. Then, a larger set of samples are compressed, and the data taken from their respective films is used to create an input for the regression learner. Finally, a third set of samples are compressed, and their pressure paper is ultimately used to test the accuracy of the model.

3.1 Material Selection

The material selected for this experiment was Amazon Basic's ABS. The reason why is because ABS plastic is one of the most common 3D printing materials available to consumers (ALT LLC, n.d.) in addition to its low price point and strength. With the purpose of this experiment being to develop a method to predict 3D printed object behavior, the material selection was not critical. The only constraint was that it needed to be a plastic FDM material. Experimenting with AM plastic materials was desirable due its relatively low cost when compared to metal printing (Gregurić, 2019).

3.2 3D Printed Samples

The next step in the process was to determine the geometric characteristics of the samples to be used for the experiment. To perform this experiment there needed to be samples for creating and testing the ML regression model. Ultimately, four cylinders were selected for creating the model. These four cylinders only varied by height and diameter. All other characteristics of the cylinders were the same including their full density.

Printing parameters such as temperatures, nozzle speed, and layer height, the parameters that would be used for all samples in the experiment needed to be determined. Through trial and error, a set of parameters was chosen that created a

satisfactory part. The slicing software used for this experiment was the Cura-Lulzbot 3.6.18 slicing software. The parameters used for printing can be reviewed in Appendix A:.

All samples were printed on the Lulzbot TAZ Pro 3D printer. Due to ABS filament tending to warp and delaminate when not printed in a heated atmosphere, a cardboard box was used to hold waste heat from the bed and nozzle in the enclosure. A standard 4mm corrugated cardboard box was cut and fit to enclose the printer. A small piece of acrylic was taped to one side of the box and used as a window to view the print without lifting the box. The box was set on top a table so that minimal gaps existed around the perimeter. Temperatures inside the box were not measured during the experiment, however, the build plate and nozzle temperature were 72.5 and 245 degrees Celsius respectively. Once a print was started, the box was immediately placed over the printer. The room that the parts were printed in was approximately 23 degrees Celsius with a light draft.

All samples used in this experiment were cylindrical and could be parameterized as illustrated in Figure 3.1 below. The variable *D* represents the diameter and the variable *H* represents the height.

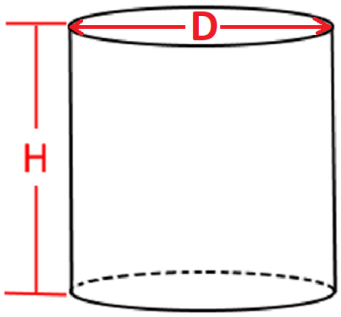

Figure 3.1: Parameterized 3D Printed Cylinder

The following list of combinations in Table 3.1 was used for printing the samples that would later create the ML regression models. Four sets of the four combinations were printed for a grand total of 16 samples used in making the model. The reason for having four identical sets was to account for repeatability in behavior of identical printed parts and for compression of a part to two separate depths.

Table 3.1: Dimension Combinations for Model Creating Samples

Dimension Values (in.)	
Diameter	**Height**

1	2
1	4
2	2
2	4

Dimension combinations used for printing parts to test the model can be seen below in Table 3.2. The sample justification column describes the intention that the sample height and diameter will have on the trained ML regression models. The word unseen is used to describe a dimensions exposure to the trained models. Since all the ML regression models were built using only samples with 1 and 2 inch diameters as well as 2 and 4 inch heights, it could be said that these dimensions have been seen by the regression models. However, using a diameter such as 2.25 inches, or a height of 0.75 inches would both be inputs that the models have not seen.

Table 3.2: Dimension Combination for Model Testing Samples

	Dimension Values [in.]	
Sample Justification	**Diameter**	**Height**
seen diameter, unseen height	1	1
seen diameter, unseen height	1	5
unseen diameter, seen height	0.75	2
unseen diameter, seen height	1.5	2
unseen diameter, seen height	2.25	2
unseen dimensions	1.5	3
unseen dimensions	2.25	0.75
unseen dimensions	0.75	0.75

Copies of model testing samples were not made. To better visualize the entire sample body, a Sankey Diagram was created as a visual aid. Figure 3.2 below shows this diagram with the number of samples represented in parenthesis.

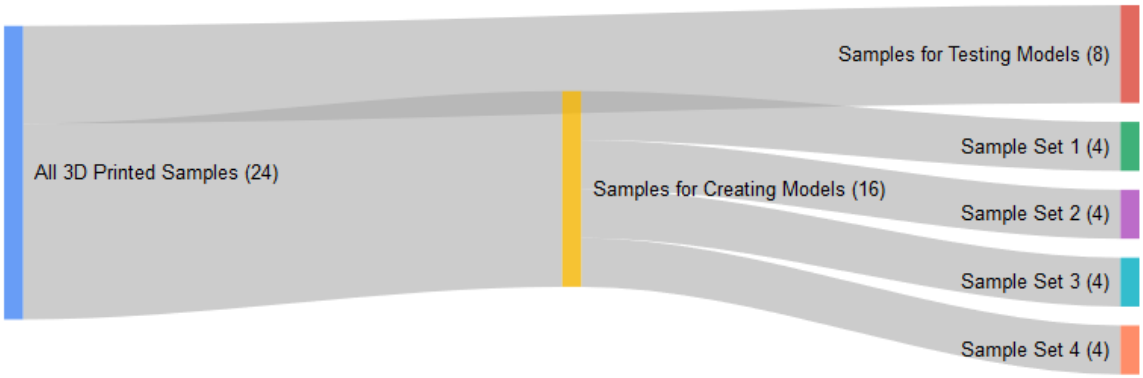

Figure 3.2: Samples Used in Creating and Testing the Regression Learner

3.3 Pressure Paper

The pressure paper chosen is Fujifilm's Prescale MS which can measure pressures ranging between 10-50 MPa. This paper is well respected within the manufacturing industry and is commonly used to measure phenomena including, but not limited to, gasket loading, parallelism of rollers, and non-uniform die contact. The film works by placing it in between 2 surfaces and applying a load. The resulting pressure will develop the film by bursting microcapsules that lie within. Microcapsules inside the film rupture at a specified pressure and mix with a layer of color developing material. The greater the pressure, the more intense the color appears on the paper. The paper takes 60 minutes to fully develop after loading. The film can be used in two different ways: standard continuous pressure or standard momentary pressure. With standard continuous pressure the pressure is loaded over two minutes, held for two minutes, then released. With momentary pressure the pressure is loaded over five seconds, held for five seconds, then released. This experiment was performed using the continuous pressure conditions. The results, which vary depending on the temperature and relative humidity of the testing environment, can be interpreted with a chart provided by the manufacturer (Fujifilm, n.d.).

The purpose of this film was to obtain an analyzable pressure distribution that occurs at the interface between the plastic cylinders and a hard steel surface. A simplified test apparatus schematic can be reviewed in Figure 3.3. Compression testing for this experiment was done in an environment with a temperature of 24.4 degree Celsius and a relative humidity of 22.5%.

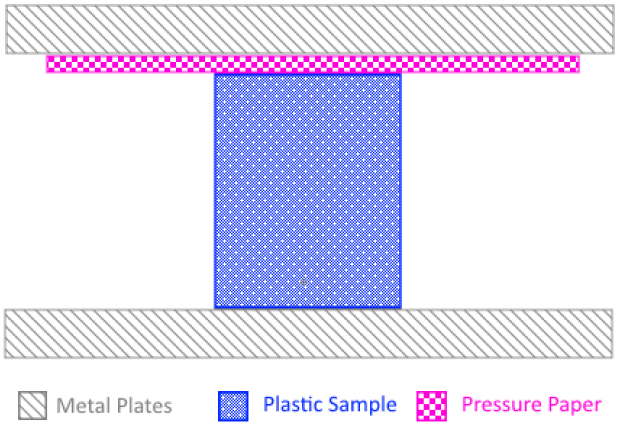

Figure 3.3: Testing Apparatus Schematic

3.4 Testing Apparatus

The testing apparatus will consist of an Instron 5500 loaded with a 150 kN load cell. In between the load cell and the base of the Instron are two metal plates, the FujiFilm pressure paper, and the 3D printed cylinder. The cylinder is centered in the apparatus using a jig that ensures the center of the cylinder lies vertically colinear with the plates being used to compress it. The pressure paper always contacted the top of the cylinder with respect to the build orientation. The purpose of using the Instron vs a servo press is to more accurately measure the force and displacement of the slide. Figure 3.4 below shows the testing apparatus in use.

Figure 3.4: Testing Apparatus

3.5 Image Processing

The purpose of the image processing code was to extract quantifiable data from the Fujifilm Prescale that could be used to train a regression learner in MATLAB. The first step to analyzing the pressure paper was to scan the papers into a digital form. The papers were scanned using a Color LaserJet Enterprise Flow MFP M681 flatbed scanner set to output the scan as a 24-bit TIF image with a 600 dot per inch (dpi) resolution. A 24-bit TIF uses an RGB color band, which is different than a 32 bit TIF which uses a CMYK color band. MATLAB image processing toolbox was unable to directly convert 4-channel images to grayscale, so to avoid unnecessary conversions the 24-bit TIF was selected.

Once scanned, the digital images were cropped into a 1:1 aspect ratio and rotated so that the infill lines were oriented perfectly horizontally. This editing was performed in the Windows photo viewing app for Windows 10. An illustration of the editing process can be reviewed in Figure 3.5.

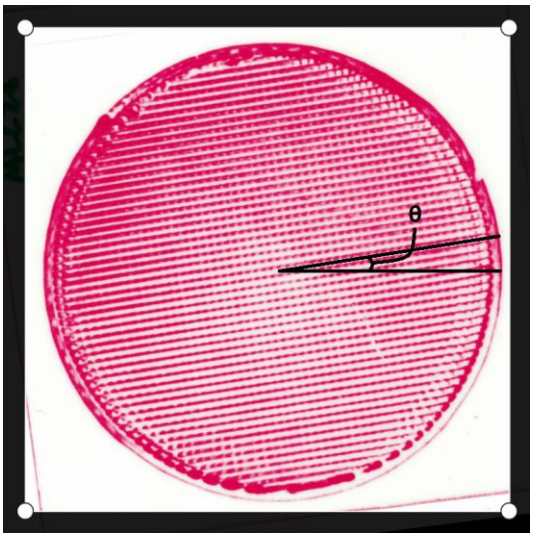

Figure 3.5: Photo Cropping and Rotating a Ø 2.0" Sample

An extra detail considered when rotating the image was to make sure the starting point of the print layer was in one of two places: either the top left or top right. The location of that point was not able to be controlled due to it not being an automatically generated location in the slicing software. The starting point for each layer was constant for each sample. Consistent layer starting positions create a vertical channel as shown in the front of the cylinder in Figure 3.6. The two locations of the starting positions can be seen circled in orange below in Figure 3.7.

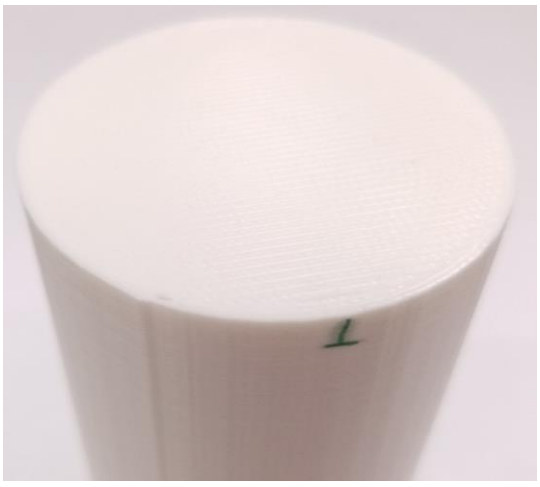

Figure 3.6: Vertical Channel Created by Layer Start Point on a Ø 1.0" Sample

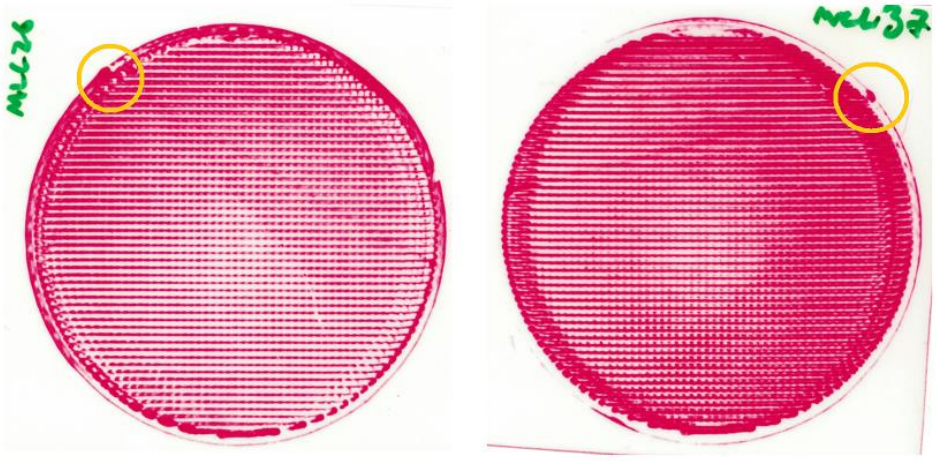

Figure 3.7: Upper Left Starting Point (Left) Upper Right Starting Points (Right) (Ø 2.25" Samples)

The cropped and rotated images were then uploaded to a custom MATLAB code. The area of interest (AOI) for this code was always the region that developed due to the printed cylinder face compressing the pressure paper. The code was programmed to perform the following tasks:

1. Import image
2. Convert image to grayscale
3. Use Otsu method for image thresholding to select AOI
4. Create a mask of AOI by locating disk shaped morphological objects within binary image and storing them as structured objects
5. Create circle centered at the centroid of the AOI with a diameter equal to the average height and width of the AOI
6. Find all points inside circle that contact the AOI
7. Select and plot 1000 data points from step 6
8. Export all useful information from each point in a tabulated text file
9. Repeat for all images

To further expand, Otsu's method is an algorithm that can separate pixels across an image into one of two categories, foreground or background. The threshold of where to draw the line between pixel intensity can be varied to capture the entire region of interest (Otsu, 1979). The output from this image manipulation is of the binary file type. MATLAB's *strel* command is utilized to create morphological structuring elements. Next, the *imerode* function is used to perform multiple binary erosions on the image by using all structing elements of the original image in succession to calibrate the regions. All pixel regions less than a specified value are converted to

logical values that can then be manipulated mathematically. More simply put, locations on the image that are not close to contacting one another are defined as separate regions that can be called out for future reference. For an example, the processes described immediately above were applied to the image in Figure 3.5. Figure 3.8 shows the image converted to binary using the Otsu method. The regions of the image are defined by MATLAB in a structure matrix.

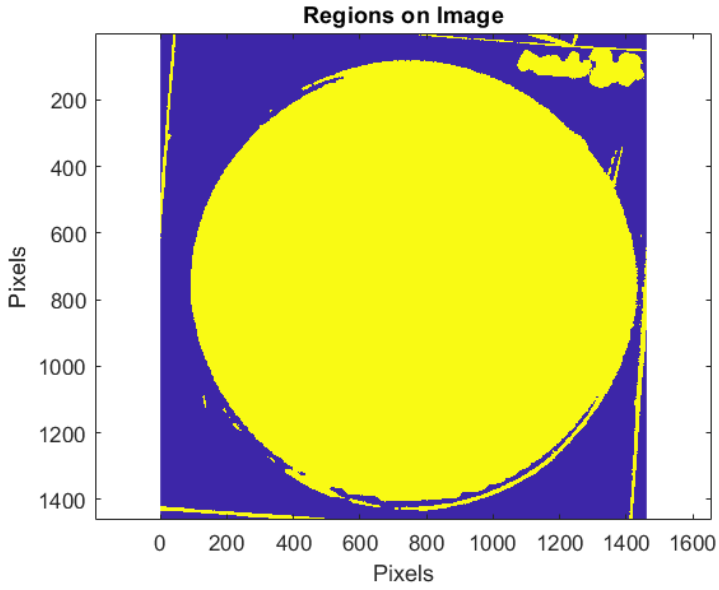

Figure 3.8: Regions of Image Segmented

For these images, the offset value was adjusted to fully capture the region with the largest area (the AOI). This area was selected to create a mask. The final mask can be seen below in Figure 3.9.

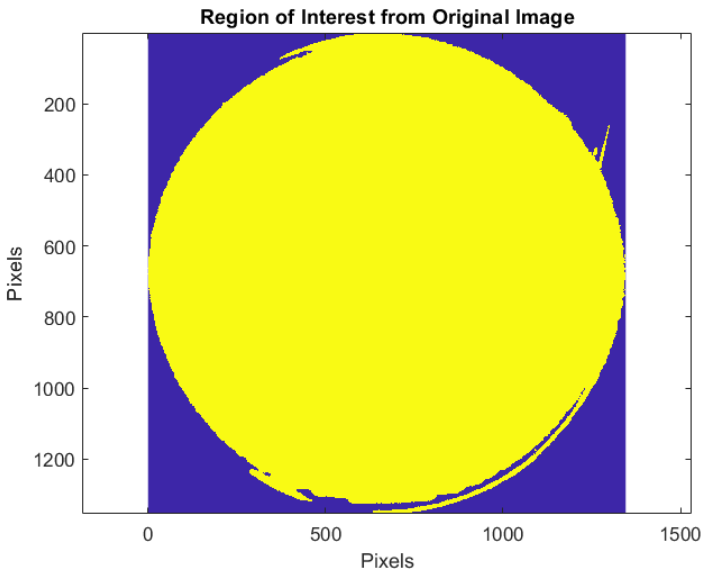

Figure 3.9: AOI Cropped from Original Image using Otsu's Offset Method

From this image, the height and width dimensions were taken, averaged, and used as the diameter of the circle that would be used to capture data points. This circle was centered around the centroid of the image which was automatically calculated. The centroid was weighted by pixel density within the AOI. It was important to adjust the offset value to obtain a mask region as close to a perfect circle as possible. A circle was drawn on the face of the image and all points within the circle were plotted as a blue dot on the masked image. This can be seen below in Figure 3.10. Due to the high image resolution it is difficult to distinguish the blue dots from one another.

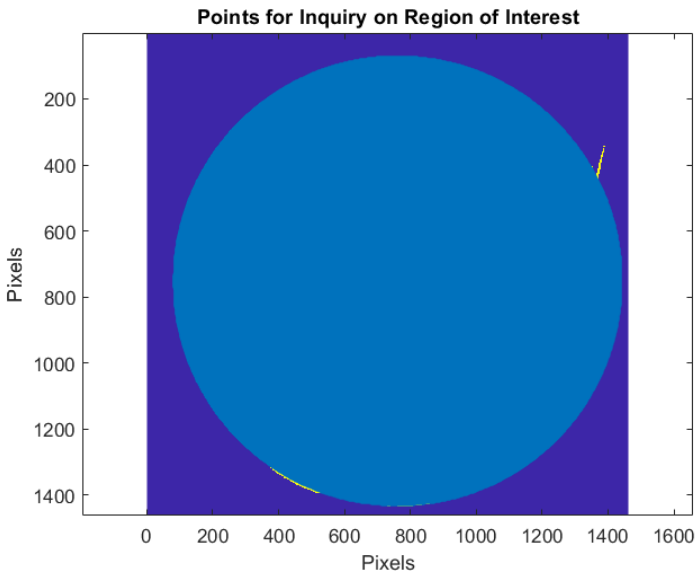

Figure 3.10: Potential Data Points Inside the AOI

The final visual product of the image processing code can be found in Figure 3.11. The figure shows a heatmap of the different intensities of the grayscale image. The large red ring around the circle designates the area in which random points can be selected. The randomly selected points within this circle are shown as red dots.

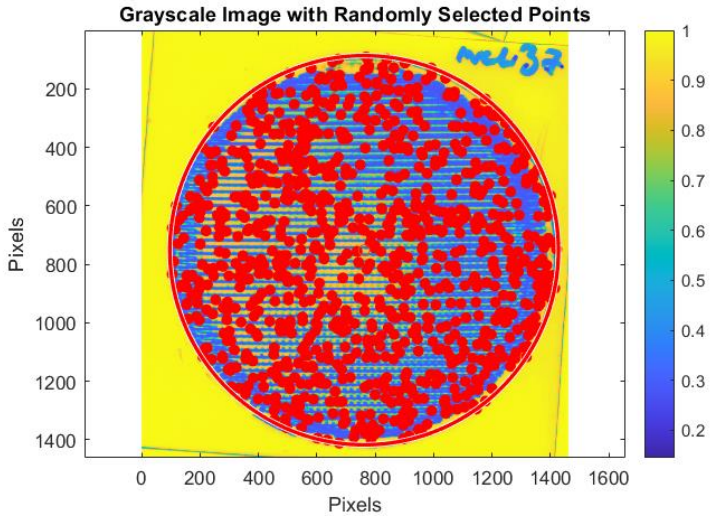

Figure 3.11: Processed Image with Randomly Selected Points

Each dot had the following information exported from it:

- Row distance from centroid[in]
- Column distance from centroid [in]
- Distance to outer edge [in]
- Grayscale intensity value
- Theoretical diameter of the sample [in]
- Measured diameter of the sample [in]
- Theoretical height of the sample [in]
- Measured height of the sample [in]
- Compression depth [in]
- Compression cycle number

This information will be used as the inputs for the ML regression learners. The ten bullet points listed above are referred to as dimensions when inputting them together in a row as a single data point.

3.6 Image Matrix Conversions

This section covers the methods used for converting the image data after it was imported into MATLAB as a TIF. TIF files can easily be manipulated in the same way that any other matrix could since each pixel in the photo represents a value in the matrix. The image was scanned at 600 dpi. The assumption was made that an array of 600 pixels was equivalent to 1 inch. This assumption was justifiable due to the extremely proximity that the laser scanner captured the image at. In the previous section, the scanning process was discussed as well as the conversion of the TIF file to grayscale. This section will discuss how the image files were converted from grayscale to density, and from density to pressure.

For reader clarification, when the word density is used it is referring to the degree of pinkness of the pressure paper once it develops. Density values fall within a numeric range of 0 to 1.5 and a visual range of white to pink. When the word intensity is used it is referring to the grayscale value of the image being processed in MATLAB. Intensity values fall within a numeric range of 0 to 1 and a visual range of black to white respectively.

3.6.1 Converting Grayscale to Density

The packet that came with the pressure paper included a scale to correlate the density of the pressure paper to physical numbers that ranged on a scale from 0 to 1.5. For a better visualization, Figure 3.12 below shows the scale (rotated 90° counterclockwise) that was provided with the paper. All images involved in this experiment were scanned by the same scanner and with the same resolution and file type.

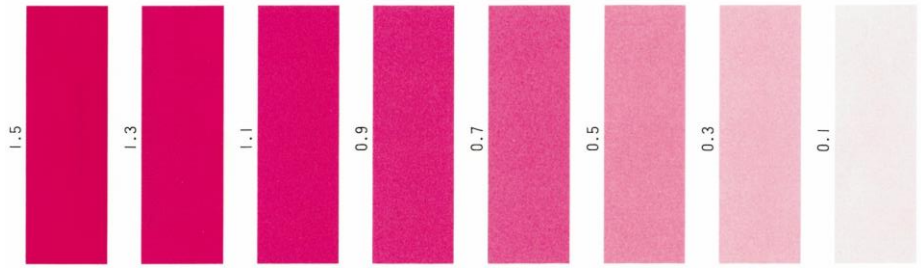

Figure 3.12: Density Scale from Fujifilm

The process of correlating the grayscale values to densities went as follows. First, the image was converted to grayscale. Applying a grayscale filter to the image converted the original image to intensity values. Then, using a click and drag rectangular mask function, a bar on the scale was cropped out as shown in Figure 3.13.

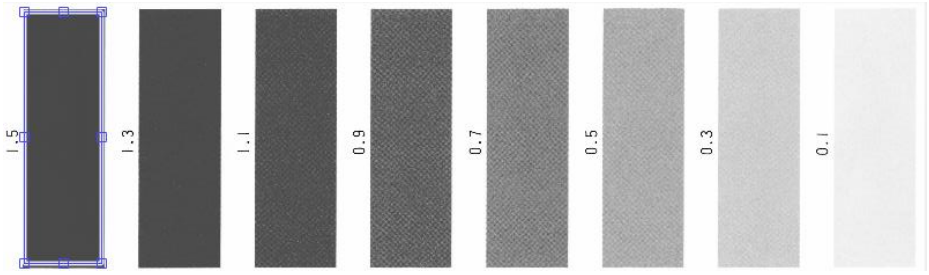

Figure 3.13: Density Scale Converted to Intensity with Cropped Region

The cropped region was then replotted as a binary mask over the image. A binary mask sets all pixel values outside the mask region equal to zero, and all pixel values inside the mask region equal to one. The mask was then multiplied to the original image to obtain the original grayscale values of the cropped region as shown in Figure 3.14.

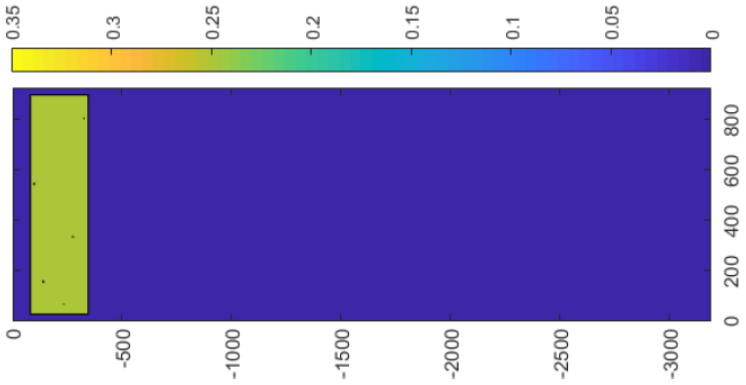

Figure 3.14: Image Mask of Cropped Region

Finally, the code took the arithmetic mean of all non-zero values within the image. This process was repeated with all bars on the scale. The density and grayscale values were then plotted with each other in Excel to obtain an equation relating density as a function of grayscale values. This relationship can be seen plotted in Figure 3.15.

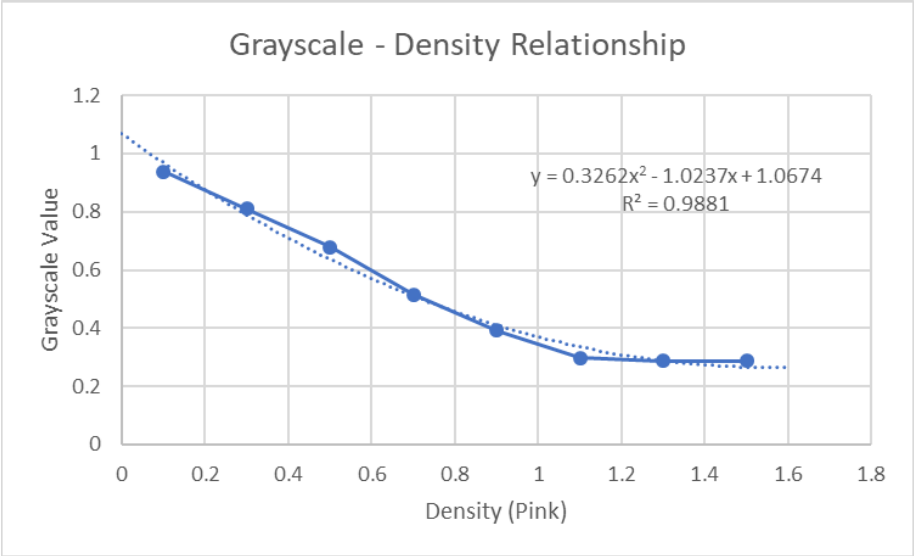

Figure 3.15: Grayscale - Density Relationship

3.6.2 Converting Density to Pressure

Two lines were given by the manufacturer to relate density to pressure: line A and line B. Choosing the correct line to use involved measuring the temperature and humidity of the environment that the pressure paper was pressurized and developed in. The chart that displays the conditions for each line can be seen in Figure 3.16. Any combination of humidity and temperature that falls above the line means that condition A is to be used. Any combination of humidity and temperature that fall

below the line means that condition B is to be used. The values of this graph were extracted from the packet using a program called Plot Digitizer.

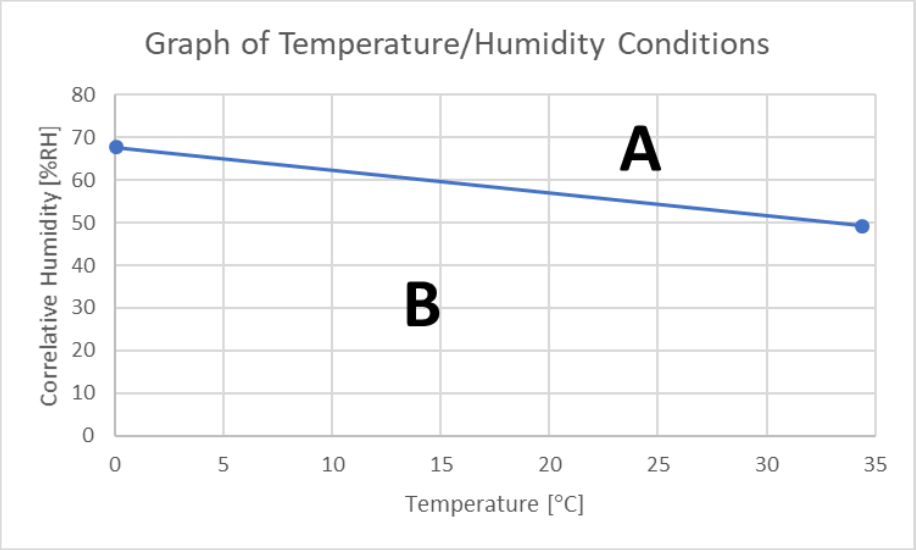

Figure 3.16: Graph of Temperature/Humidity Conditions

With the conditions for choosing a line known, the pressure versus density lines could be extracted. Since the conditions of the testing environment could not be predicted, both lines were extracted from the packet. The graphs of line A and B can be found in Figures Figure 3.17 and Figure 3.18 respectively.

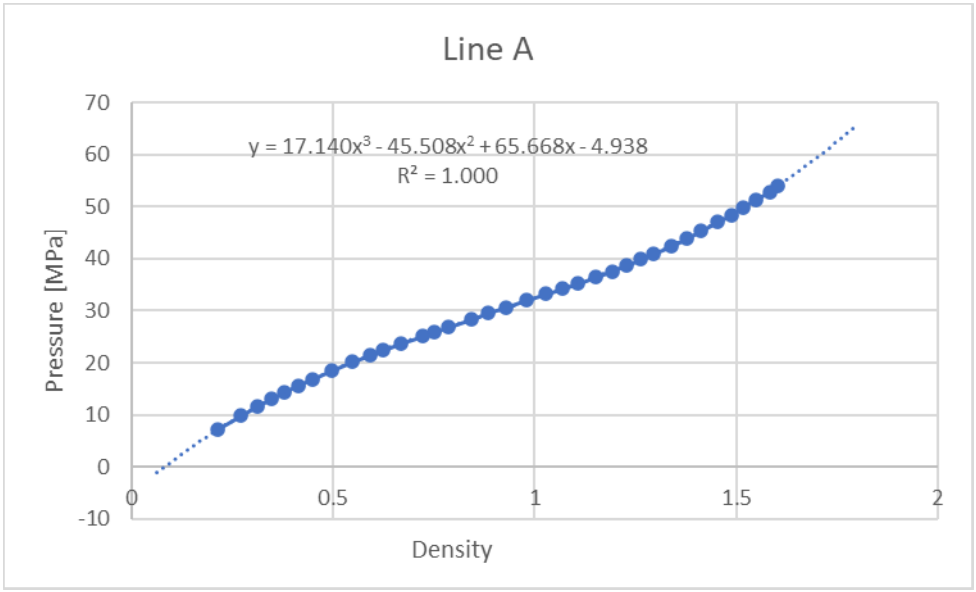

Figure 3.17: Density vs Pressure for Line A

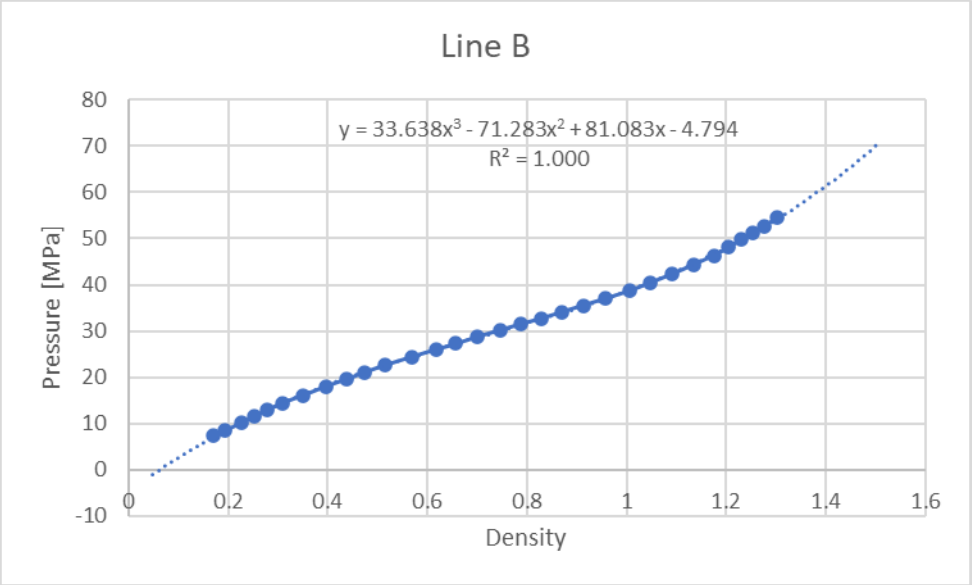

Figure 3.18: Density vs Pressure for Line B

A trendline was fit to both lines, and the equations of the lines were used in the image processing code to convert the densities to pressures. Forecasting was used ahead and behind the data points to ensure that the trendlines did not diverge from their expected paths.

Grayscale values need to fall within a certain range to avoid error, a chart was made to analyze the distribution as shown in Table 3.3. This chart combines information from the previous section to display the relationships between the grayscale intensity measured from the images, the grayscale values calculated using the equation of the trendline, density values, and both pressure A and B. The acceptable ranges of pressures can be seen highlighted in dark yellow.

Table 3.3: Density to Pressure Conversion Chart

Grayscale Intensity (Measured from Image)	Grayscale Intensity (Trendline)	Density (Pink)	Pressure A	Pressure B
0.94	0.97	0.10	1.19	2.71
	0.88	0.20	6.51	**8.98**
0.81	0.79	0.30	**11.13**	**14.24**
	0.71	0.40	**15.14**	**18.67**
0.68	0.64	0.50	**18.66**	**22.49**
	0.57	0.60	**21.78**	**25.89**
0.52	0.51	0.70	**24.61**	**29.08**
	0.46	0.80	**27.25**	**32.25**
0.39	0.41	0.90	**29.80**	**35.61**
	0.37	1.00	**32.36**	**39.36**
0.30	0.34	1.10	**35.05**	**43.71**
	0.31	1.20	**37.95**	**48.85**
0.29	0.29	1.30	**41.18**	54.98
	0.27	1.40	**44.83**	62.32
0.29	0.27	1.50	**49.02**	71.05

3.7 Compression Depth Determination

Fujifilm Prescale works best inside a certain range of pressure; a pressure too high or too low would mean that while some papers developed nicely, others would potentially not develop at all, or would develop too intensely. Different sample heights and contact surface areas would create a wide range of values on the

pressure paper if they were all compressed to the same depth. Therefore, each sample had a different range of compression associated with it.

To begin, one copy of the four samples being used to create the ML model were printed. The sole purpose of these samples was to compress them multiple times to different depths and extract useful information from the pressure paper being used with them. Material relaxation due to cyclic loading was ignored for these tests. The samples were loaded into the Instron and compressed anywhere between 10 to 150 thousandths of an inch. Compression depth ranges were somewhat subjective. The pressure papers were compared to the given density scales to determine whether a deeper or shallower compression would be useful.

Once all samples were compressed through various ranges, the papers were scanned and masked using the same procedure as explained in the beginning of section 3.5: Image Processing. With the image mask capturing the area of interest, a histogram was made of all values inside the mask. This showed the distribution of grayscale values inside the AOI. Compression ranges were chosen by finding the limits at which the peak of the normal distribution stayed inside the acceptable range. An example of the histograms being described can be found below in Figure 3.19. This figure shows how the distribution of pixel intensities inside the AOI change based on varying compression depths.

Compression Depth [in]	Histogram	Original Photo
25/1000	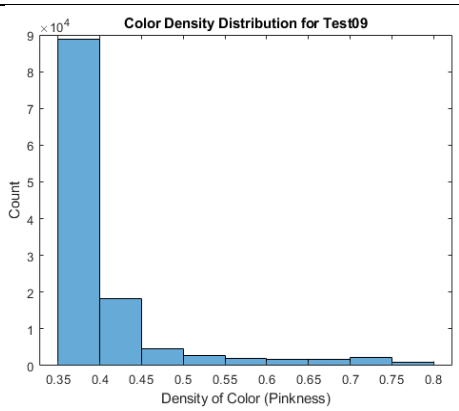	
75/1000	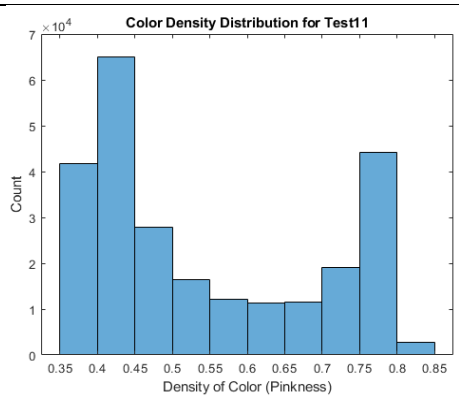	
125/1000	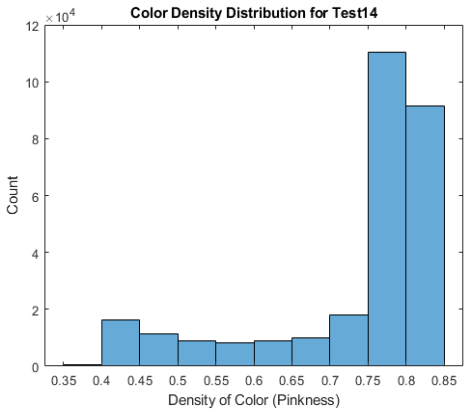	

Figure 3.19: Compression Histograms from Sample 12F

Ultimately each sample was compressed to the same depth 5 times. The testing was performed in temperature/humidity condition B. The histograms were analyzed for

each compression and the final two compression depths used for each sample can be found listed in Table 3.4.

Table 3.4: Sample Compression Depths Chosen for Model Creation Samples

Sample Dimensions [in]		**Testing Compression Depth [in]**	
Radius	**Height**	**Low Depth**	**High Depth**
1.000	2.000	0.050	0.125
1.000	4.000	0.075	0.125
2.000	2.000	0.050	0.100
2.000	4.000	0.075	0.150

Samples used solely for testing the model did not have their compression ranges tested, rather good engineering judgement was used. The images were sampled and analyzed with the histogram code to ensure that they did not exceed acceptable bounds. The ranges used for the model testing samples can be seen below in Table 3.5.

Table 3.5: Sample Compression Depths Chosen for Model Testing Samples

Sample Dimensions [in]		
Radius	**Height**	**Testing Compression Depth [in]**
1.000	1.000	0.075
1.000	3.000	0.085
1.000	5.000	0.125
0.750	2.000	0.100
1.500	2.000	0.100
2.250	2.000	0.075
0.750	0.750	0.05
2.250	0.750	0.075
1.5	3	0.100

3.8 Data Compiling for Machine Learner Creation and Testing

Three tables were used for machine learning. One table was used to create the models and two tables were used to test the models. Each data point had 9 dimensions. The dimensions for each data point were listed in columns. Since it was desired to test the models predicting ability of compression depth and grayscale value, one of the testing tables needed the grayscale dimension to be empty, and one of the testing tables needed the compression depth dimension to be empty. The

pressure column was omitted from all tables. Since curve fitting was used to approximate pressure, keeping the pressure column would only add error to predicting compression depth. As for predicting grayscale, the model would be able to see a direct correlation of the grayscale value to the pressure since pressure is a function of grayscale value. The model creation sheet contained all information listed at the end of section 3.5.

Data was not recorded for every cycle for each sample. Five cycles of the 1 inch diameter and 3 inch high sample that was used to test the ML regressions were omitted due to user error. One cycle from the 2 inch diameter by 4 inch high sample used to create the ML regressions was omitted due to machine error.

As stated before, 1000 data points were taken on each pressure paper sheet. For the model creation samples, 200 data points were taken out in order to be used for testing the model. This means that 800 of the 1000 data points taken for model creation pressure paper samples were used to create the model. This was done because it was desired to see if there was any difference between the model's ability to predict values on samples with dimensions that it was seen before versus samples that it has not.

For creating the model, 79 pressure papers, each having 800 data points were used in the model creation table. This gave a total of 63,200 inputs to the machine learner to create the models ([79 samples × 800 data points]).

For testing the model, 200 data points from each of the 79 samples used to create the model were used to test the model along with 1000 data points from the 40 samples used solely for testing the models. This gave a total of 55,800 inputs to test the models ([79 samples × 200 data points] + [40 samples × 1000 data points]). A grand total of 119,000 data points used in this experiment.

3.9 Creating Machine Learning Regression Models

Two results were desired to be predicted: compression depth and grayscale value. To predict these, a table containing the listed information for each sample at the end of section 3.5 was compiled to be used as inputs for the models. To test and see if model validation types affected the results of the ML models a 10% hold out validation, 25% hold out validation, and 3 fold cross validation model were used to test the model for predicting either variable. For the six variable and model

validation combinations, 19 different ML regression models were trained using the 63,200 inputs for creating the model.

Hold out validations set aside a percentage of the body of input to test the accuracy of the model after the model is built to understand the accuracy of any model. K-fold validation models act as described in section 2.5.8, and divide the sample body into groups that are compared to one another.

3.10 Testing the Machine Learning Regression Models

There were two dimensions that would be predicted; grayscale and compression depth. Each dimension would be predicted using three different validation types; 25% hold out validation , 10% hold out validation, and 3-fold cross-validation. Each model had a different combination of intended variable for prediction and validation type. These combinations can be found below in Figure 3.20.

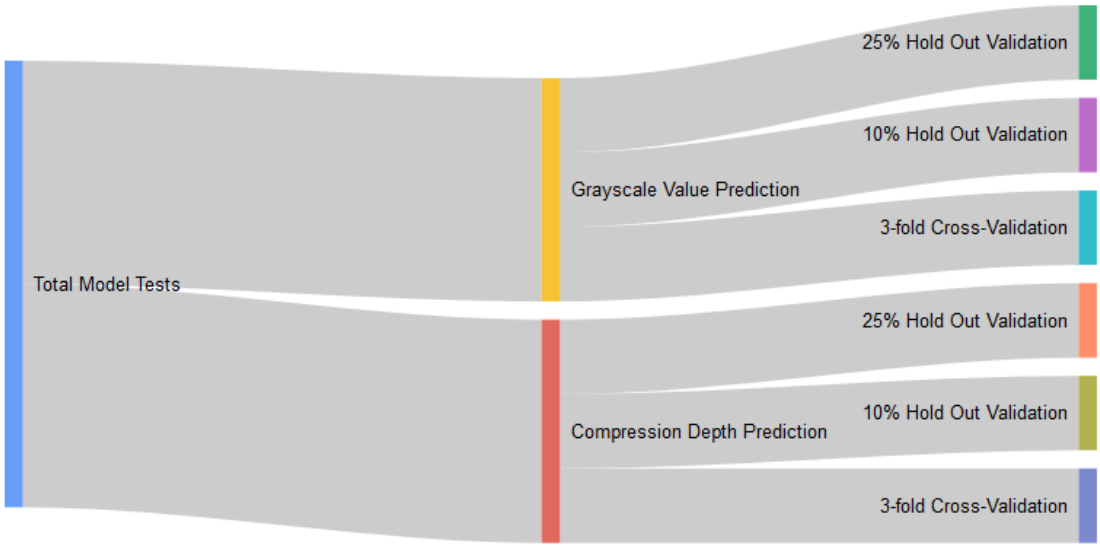

Figure 3.20: ML Model Variables to be Predicted and Validation Types

Every validation type consisted of 19 regression models. These were the trained models that would be used to predict the deformation or grayscale value. Each of the regression models were trained using 55,800.

3.11 Testing Prediction Accuracy of ML Regression Models

Plotting residual error of the sample outputs and comparing them visually to find the best models is not practical, so a more mathematical approach was taken. It was

determined that computing the root mean square error (RMSE) of the residual errors would be the best metric to compare the accuracy of the regression models. Residual error is the difference between the actual value of a point and the predicted value of a point. The RMSE is a measure of the standard deviation of the residual errors, which indicates how spread out the residuals are. The equation for RMSE can be found below in Equation 3-1.

$$RMSE = \sqrt{\frac{1}{N}\sum_{i=1}^{N}(y_{p_i} - y_{a_i})^2} \quad 3\text{-}1$$

Where y_p is the value predicted by the regression model, y_a is the measured value, N is the number of data points for any sample output, and i is an indexing number.

CHAPTER 4

RESULTS & ANALYSIS

The goal of the results was to determine the following:

1. Do certain validation types improve regression model accuracy?
2. Which regression model is best for predicting:
    a. Entire body of data
    b. Data with heights and diameters that the model has previously seen
    c. Data with only diameters that the model has previously seen
    d. Data with only heights that the model has previously seen
    e. Data with no heights or diameters that the model has previously seen
3. How does error vary across sample faces?

It should be noted that residual error, RMSE, and standard deviation of RMSE's all hold the grayscale which ranges from 0 to 1 for grayscale prediction and inches for compression depth prediction.

4.1 Grayscale Value Prediction Results

4.1.1 Validation Model Type Comparison

Part of training the regression models requires using a portion of the data to test against itself (hold out) or dividing the data into groups to test against themselves (cross validation). The residual error between the trained model's predictions and the real values produce a RMSE in the trainer . This RMSE is for the user to have as a gauge for how well each model performed. This RMSE is calculated by the trainers were logged in a separate spreadsheet for each validation type and regression model combination. These RMSE values were arranged in a table and interestingly the lowest RMSE for each validation model was obtained through the bagged trees regression model. Additionally, there was no significant difference between the RMSE values. The RMSE values can be reviewed below in Table 4.1.

Table 4.1: Grayscale Prediction - Trainer RMSE for Bagged Trees for All Validation Types

Validation Type	Regression Model: Bagged Trees
3-fold Cross-Validation	0.14166
10% Holdout	0.13514
25% Holdout	0.14025

A full comparison between the RMSE of all validation types and regression trainer RMSE's can be viewed below in Figure 4.1.

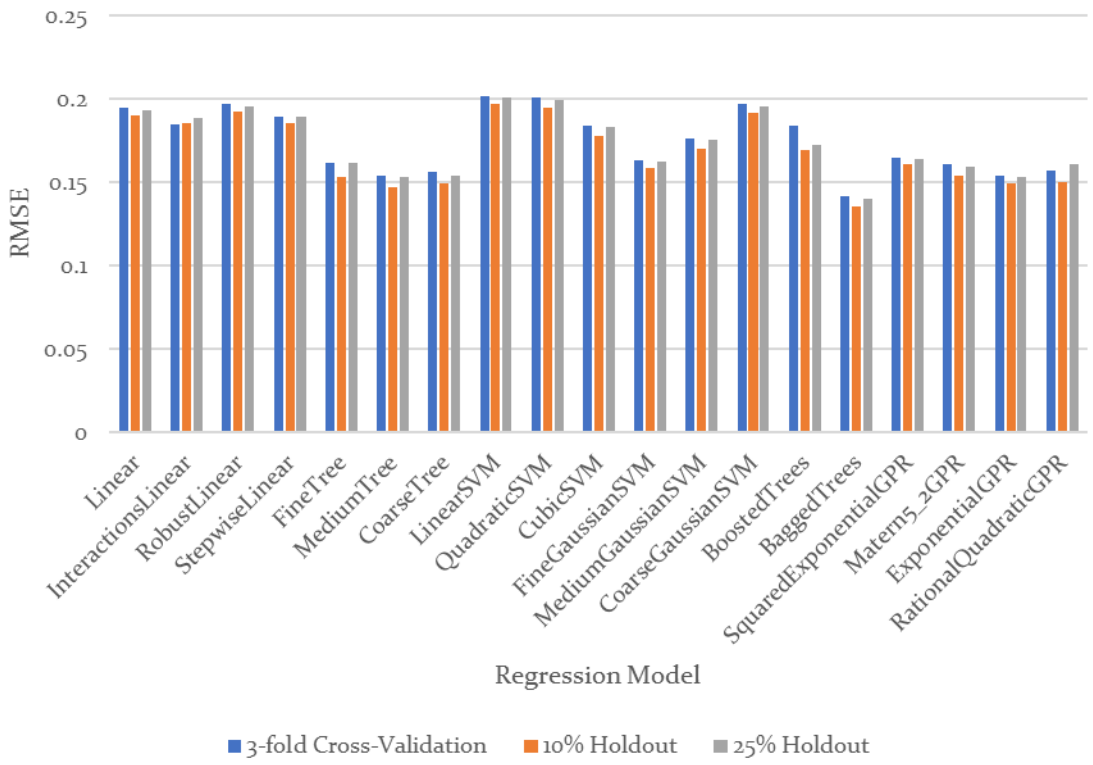

Figure 4.1: Grayscale Prediction - Validation Type and Regression Trainer RMSE

From these results it can be concluded that there is no significant difference between the validation types. For each validation type, the regression model types all have close RMSE values. However, since the 10% Holdout validation type has slightly lower RMSE values for each regression model, further comparisons will be made using it. To view the full data set, please refer to 0

Grayscale Value Training Data RMSE.

4.1.2 Determining the Best Regression Model for Grayscale Value

As outlined at the beginning of the chapter, there are five groups of data that are to be compared; the entire body of data, data with heights and diameters that the model has previously seen, data with only diameters that the model has previously seen, data with only heights that the model has previously seen, and data with no heights or diameters that the model has previously seen. The groups were made by filtering the entire body of data by heights and diameters. With there is an overlap of samples inside each group rather than each sample belonging to a single group. A sample has the possibility of being represented in up to four groups, but never all five groups. A direct comparison of the RMSE values for each data group and each regression model type can be found below in Figure 4.2.

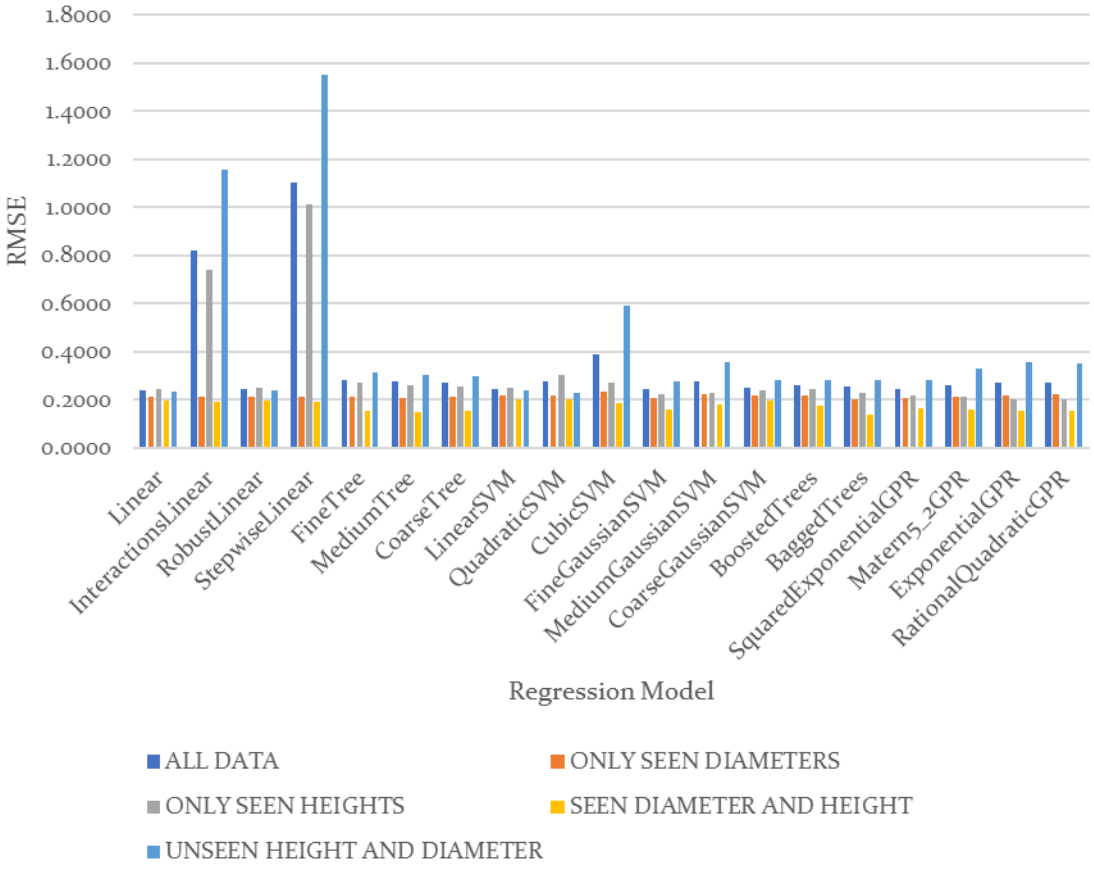

Figure 4.2: RMSE Comparison for Each Data Group and Regression Model

Most data fell below an RMSE of 0.3, and there are some very radical outliers. To narrow down the information, only the column of RSME's that hold the lowest value for each category will be further inspected. A table of this information can be found below in Table 4.2. The lowest RMSE values are outlined with a bold box. To view the full data set, please refer to Appendix C:.

Table 4.2: Grayscale Testing Data RMSE Chart for Best Models

	RMSE for Model Testing Results	Linear	Quadratic SVM	Bagged Trees	Rational Quadratic GPR
10% Hold Out Validation (10hoval)	**ALL DATA**	**0.2393**	**0.2744**	**0.2526**	**0.2690**
	ONLY SEEN DIAMETERS	0.2130	0.2163	0.2020	0.2245
	ONLY SEEN HEIGHTS	0.2426	0.3049	0.2293	0.2030
	SEEN DIAMETER AND HEIGHT	0.1961	0.2034	0.1370	0.1535
	UNSEEN HEIGHT AND DIAMETER	0.2341	0.2302	0.2818	0.3507

The most common, most basic regression model of them all, the linear regression model, was most accurate at predicting values for the entire data set. Similar accuracy can be achieved when varying only one dimension from something that the models has not seen. The Bagged Trees regression model for only seen diameters and the Rational Quadratic GPR model for only seen heights predict gray scale values with almost the same accuracy. For predicting the grayscale values for a sample with a height and diameter that the model has never seen, a Quadratic SVM model will perform best. Finally, and as expected, predicting grayscale values for samples that have both diameters and heights that the model has seen before results in the lowest RMSE and yield the most accurate results with the Bagged Trees regression model, which was the same regression model that produced the lowest RMSE value for the training data.

4.1.3 Verification of RMSE Metric Sufficiency for Grayscale

One may question whether using RMSE as a metric for comparison fully captures the behavior of the regression models. There was suspicion that a small group of high residual errors may attribute to a high RMSE of a regression model within a data set. Residual errors were plotted for each sample and for each regression model type. This produced many plots; however, it was possible to sample the plots from the group and compare output predictions for regression models that fall within the same data group. The following figure, Figure 4.3, shows the original grayscale values for sample MLC11 which had a diameter of 1 inch and a height of 5 inches which falls under the seen diameter and unseen height data group. Figure 4.4, shows

residual errors between actual and predicted data points for four different regression models ran on that sample. A negative value indicated that the regression model estimated high, and a positive value indicated the regression model estimated low.

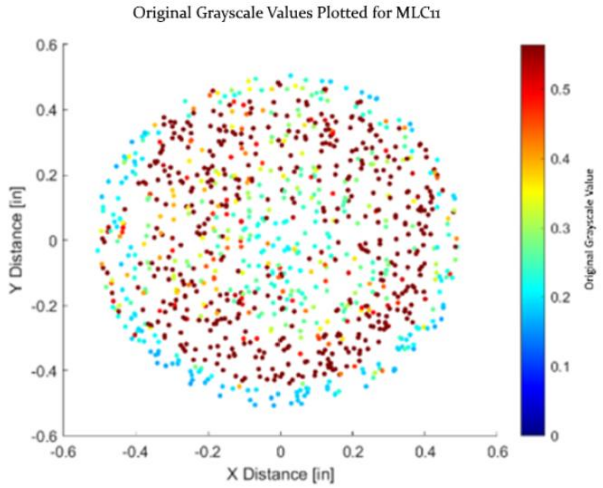

Figure 4.3: Grayscale Values Plotted for Sample MLC11

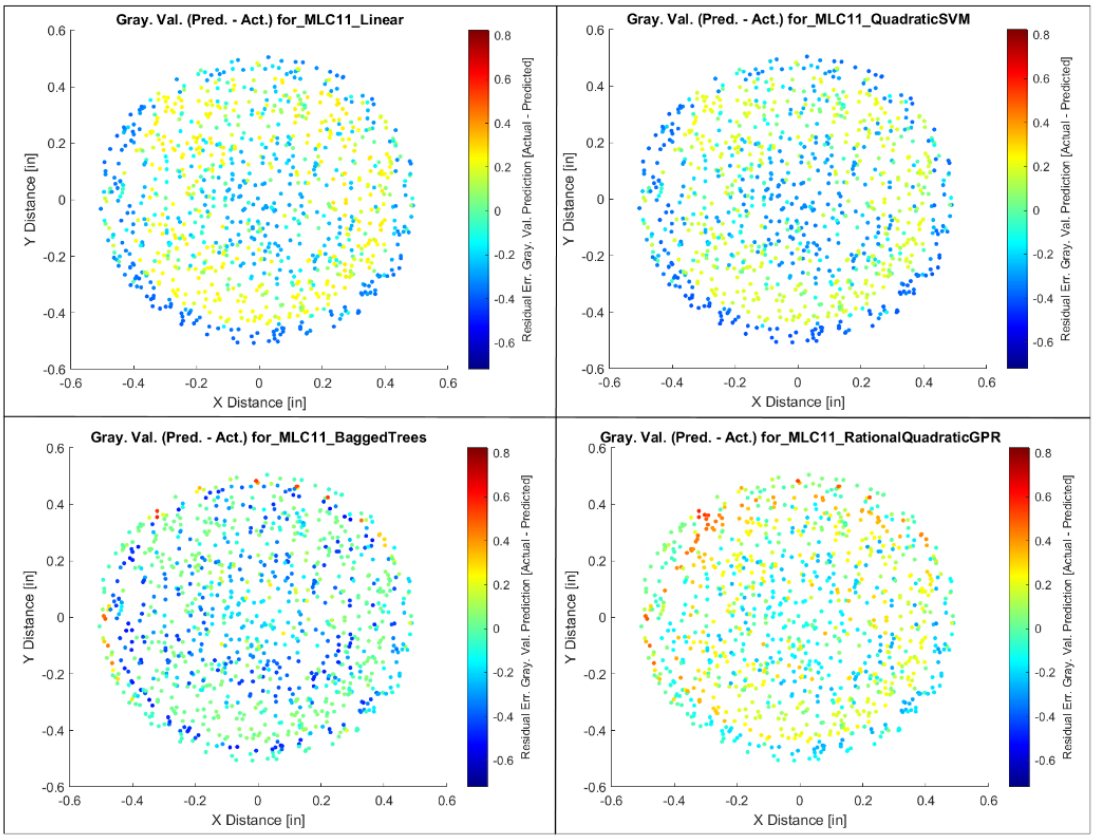

Figure 4.4: Residual Error Comparison for 4 Grayscale Regression Models

Interestingly, the start and stop point of the layer is shown through both the original grayscale value plot as well as the ML prediction plots. For this sample, the Bagged Trees regression model should yield the lowest error out of all the others. At a high level, the Bagged Trees appears to have the most data points in the green which represents values close to zero.

4.2 Compression Depth Prediction Results

Part of training the regression models requires using a portion of the data to test against itself (hold out) or dividing the data into groups to test against themselves (cross validation). This produces an RMSE in the trainer for the user to have as a gauge for how well each model performed. This RMSE is calculated automatically and was logged in a separate spreadsheet for each validation model and all the subsequent models trained within them. These RMSE values were arranged in a table and interestingly the lowest RMSE for each validation model was obtained through the bagged trees regression model for compression depth as well as the grayscale value. Additionally, there was no significant difference between the RMSE values. The RMSE values can be reviewed below in Table 4.1. It should be noted that samples for this experiment were compressed anywhere between 0.025 to 0.125 inches.

Table 4.3: Compression Depth Prediction - Trainer RMSE for Bagged Trees for All Validation Types

Validation Type	**Regression Model: Bagged Trees**
3-fold Cross-Validation	0.00102
10% Holdout	0.001018
25% Holdout	0.001056

A full comparison between the RMSE of all validation types and regression trainer RMSE's can be viewed below in Figure 4.1.

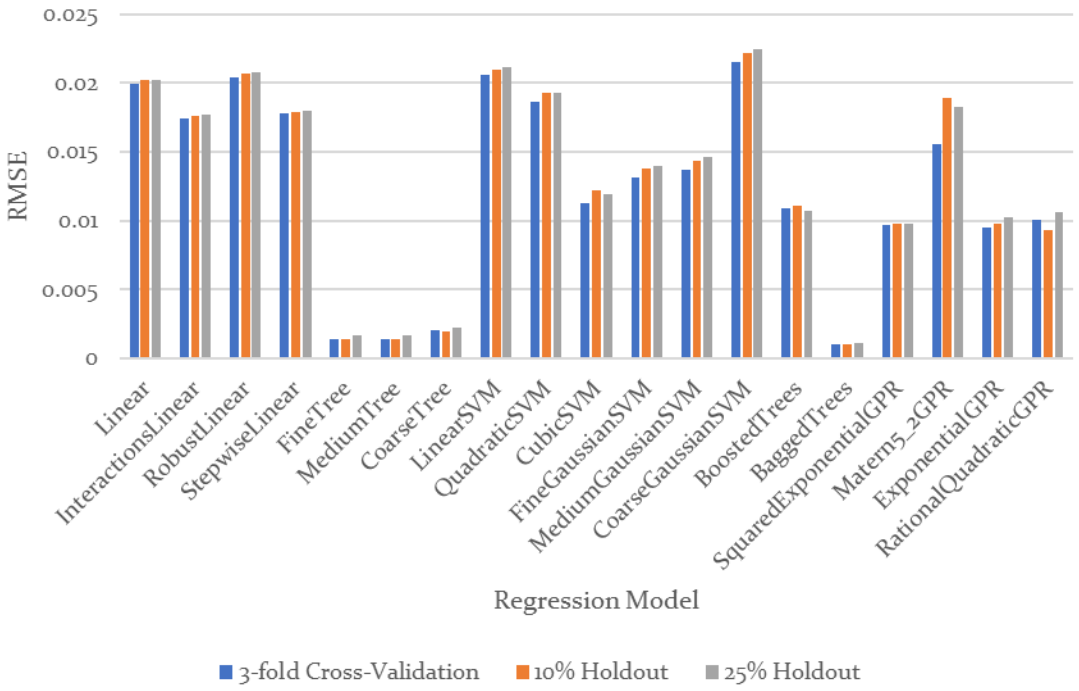

Figure 4.5: Compression Depth Prediction - Validation Type and Regression Trainer RMSE

From these results it can be concluded that there is no significant difference between the validation types. For each validation type, the regression model types all have close RMSE values. However, since the 3-fold cross-validation type has slightly lower RMSE values for each regression model, further comparisons will be made using it. To view the full data set, please refer to Appendix D: Compression Depth Training Data RMSE.

4.2.1 Determining the Best Regression Model for Compression Depth

As outlined at the beginning of the chapter, there are five groups of data that are to be compared; the entire body of data, data with heights and diameters that the model has previously seen, data with only diameters that the model has previously seen, data with only heights that the model has previously seen, and data with no heights or diameters that the model has previously seen. The four groups following the entire body of data were all created by filtering the entire body of data. With this there is an overlap of samples inside each group rather than each sample belonging to a single group. A sample has the possibility of being represented in up to four

groups, but never all five groups. A direct comparison of the RMSE values for each data group and each regression model type can be found below in Figure 4.2.

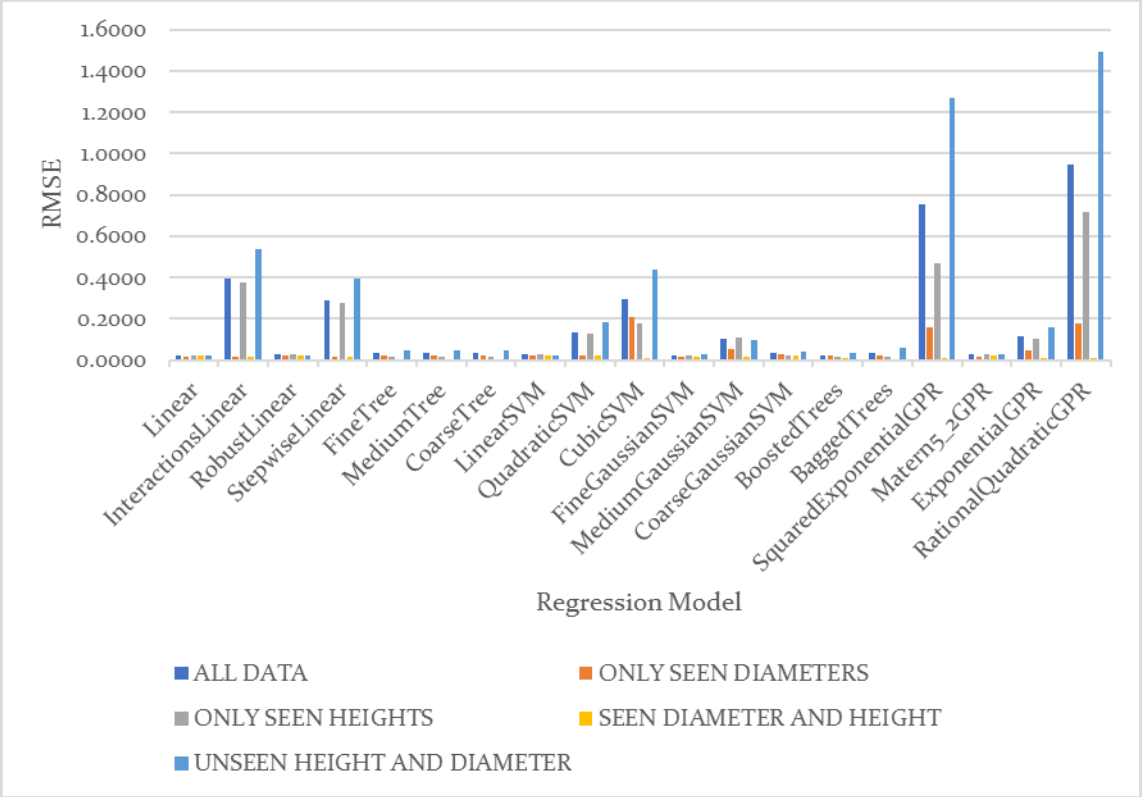

Figure 4.6: RMSE Comparison for Each Data Group and Regression Model

Most data fell below an RMSE of 0.2, but there are still some radical outliers. To narrow down the information, only the column of RSME's that hold the lowest value for each category will be further inspected. A table of this information can be found below in Table 4.2. The lowest RMSE values are outlined with a bold box. To view the full data set, please refer to Appendix E:.

Table 4.4: Compression Depth Testing Data RMSE Chart for Best Models

	RMSE for model testing results	Linear	Interactions Linear	Medium Tree	Linear SVM	Bagged Trees
3-fold Cross Validation (3fcv)	**ALL DATA**	0.0230	0.3951	0.0321	0.0250	0.0360
	ONLY SEEN DIAMETERS	0.0188	0.0165	0.0220	0.0211	0.0220
	ONLY SEEN HEIGHTS	0.0249	0.3768	0.0172	0.0275	0.0186
	SEEN DIAMETER AND HEIGHT	0.0205	0.0179	0.0017	0.0214	0.0010
	UNSEEN HEIGHT AND DIAMETER	0.0233	0.5395	0.0490	0.0225	0.0574

It is notable how the Bagged Trees model for samples with a seen diameter and height hold an RMSE like that from the training data, but other samples have an

RMSE at least an order of magnitude bigger. To not much surprise, this was an indication that the machine learner was able to predict compression depths for samples it has seen significantly better than those that it hasn't.

4.2.2 Verification of RMSE Metric Sufficiency

One may question whether using RMSE as a metric for comparison is enough to compare the accuracy of the regression models. With the suspicion that a small group of high residual errors may attribute to a high RMSE of a regression model within a data det, residual errors were plotted for each sample and for each regression model type. This produced many plots; however, it was possible to sample the plots from the group and compare output predictions for regression models that fall within the same data group. The following figure, Figure 4.4, shows residual errors between actual vs predicted data points for four different regression models. The sample tested had a 1.5 inch diameter and a 3 inch height and was compressed to 100 thousandths of an inch.

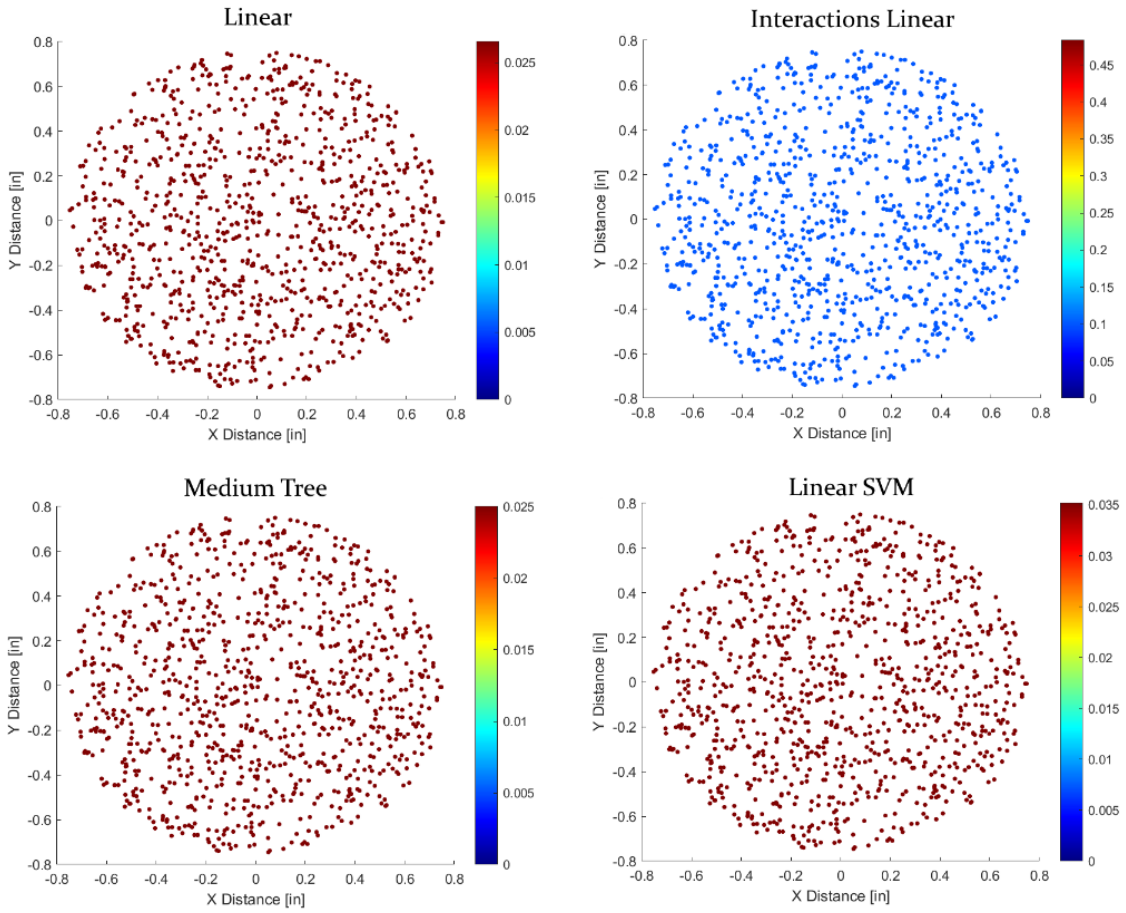

Figure 4.7: Residual Error Comparison for 4 Regression Models

It should be noted that not all scales are the same. From a high level perspective, we see that the scales for Linear, Linear SVM and Medium Tree regression models range less than that of the Interactions Linear model. Likewise, the RMSE of the for Linear, Linear SVM and Medium Tree regression models are lower than that of the Interactions Linear model. The sample plotted has both an unseen diameter and height, so it is no surprise that the Linear SVM predicted it well. It is interesting that the Interactions Linear values fall between 0.05 to 0.1 and that the Medium Tree Values all fall below 0.025. It may be an indication that samples with seen diameters have a larger influence on the predictability of compression depth than samples with only seen heights.

4.3 Variation Across Sample Faces

Variation across the sample faces can be group into three difference distributions: Annular, Flat, and Offset Annular. Annular face profiles show an axisymmetric distribution around the center of the image. Flat face profiles show all the data

points having a very similar distribution in a way that makes every data point have identical colors. These distributions come from the Decision Tree regression models. Homogenous color distributions across the graph always indicate model precision but accuracy can only be determined via the color bar. Lastly, the offset annular appears as if the center of the annular profile was shifted toward an outside edge. This creates a crescent moon shape near the outside edge furthest from the "center" of the distributions. The three face profiles can be seen below in Figure 4.8. Note that the models are plotting the residual error between the predicted values and the actual values for all points. Negative numbers mean that the model underpredicted and positive numbers mean that the model overpredicted.

A method was created to make conclusions from all the graphs. Residual error plots of compression depths and grayscale values for their respective relevant regression model types were analyzed and their profile types were recorded in a spreadsheet. This compilation enabled the body of data to be filtered into certain groups so that potential correlations could be witnessed.

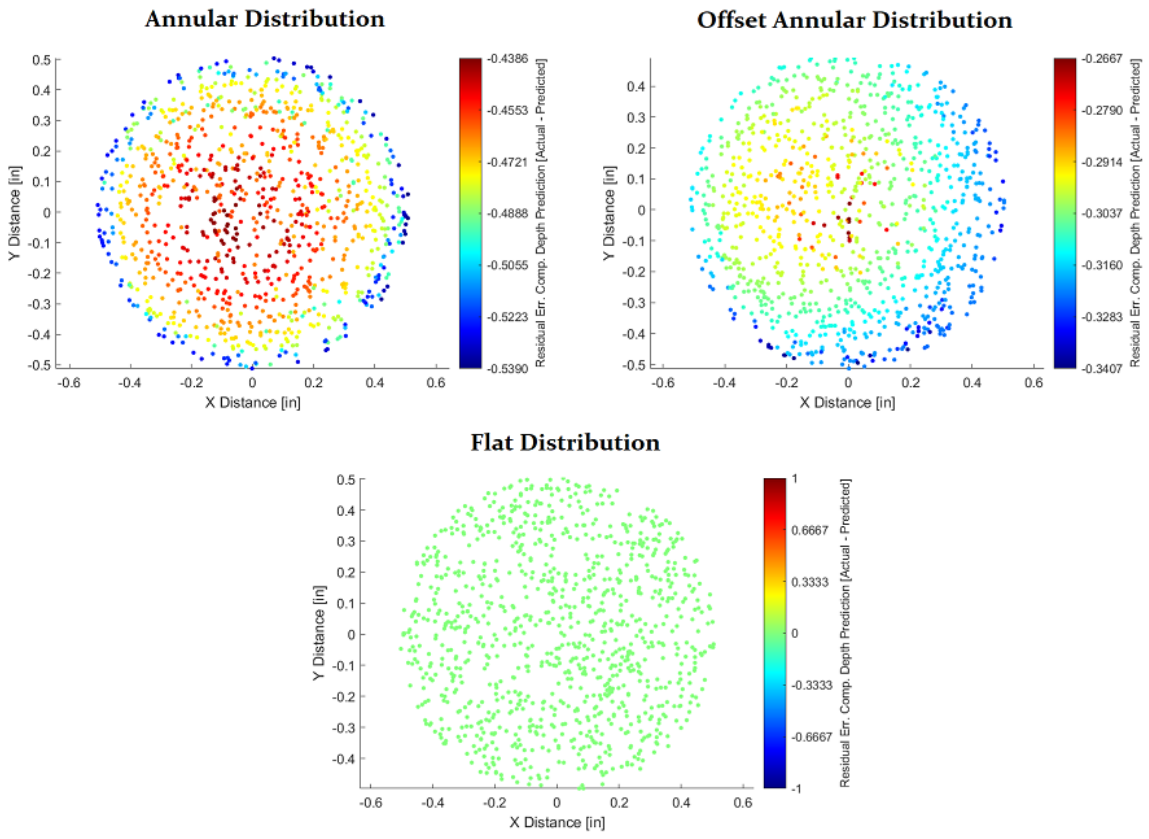

Figure 4.8: Distribution Profile Comparison

4.3.1 Grayscale Distribution Correlations

Conclusions made from reviewing the residual error plots are as follows:

- Annulus distributions are almost twice as likely to occur with a sample that has a seen height and diameter (82.3%) than one with both an unseen height and diameter (46.7%) when compared using a Linear regression model.
- There were no Flat profile distributions.
- Samples with a 0.75 inch diameter had a 0% chance of having an Annular distribution.
- Samples with a 0.75 inch height had a 30% chance of having an Annular distribution.
- Samples with a seen diameter and height that were compressed to 125, and 150 thousandths of an inch had a high chance of an Annular distribution: 95% and 100% respectively.

These correlations all come with logical explanations which are listed as follows:

- The low number of annular distributions among the unseen samples can be attributed directly to samples that had a diameter and/or height of 0.75 inches. This height is 1.25 inches lower in height and 0.25 inches smaller in diameter than the smallest dimensions of the samples used to train the models. When these samples were printed, warping occurred on the top faces which caused high variation in the pressure distribution. So, when a regression model tried to predict the distributions based solely on geometry, it likely assumed that the contact area would be like that of the samples used to train the model. This caused both over and underpredictions to occur across the face which ultimately led to a crescent moon shaped distribution. A comparison between a 0.75 inch high by 0.75 inch diameter sample and a 2 inch high by 1 inch diameter sample can be reviewed below in Figure 4.9.
- No Flat profile distributions were found due to the inputs having a high range of variability.
- Lastly, an annular distribution likelihood among the samples compressed to 125 and 150 thousandth is higher due to the higher chance of a completely circular distribution developing on the film. Each sample has a slight variation in height across it, therefore the deeper a sample is compressed, the more likely it is that the entire surface will deform and contact the pressure paper. Most samples used to build the regression models had a complete contact between the sample and the pressure paper.

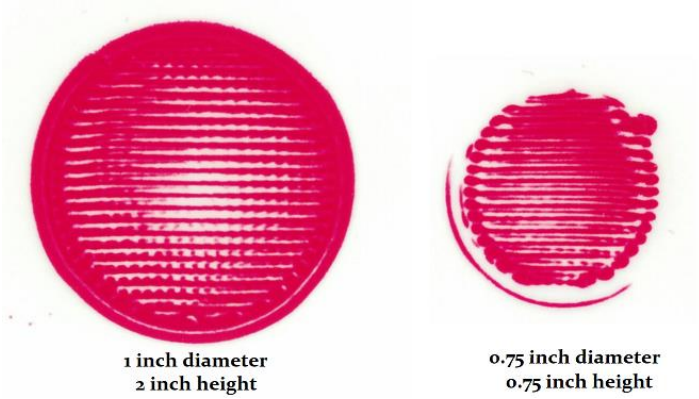

Figure 4.9: Pressure Distribution Differences

4.3.2 Compression Depth Distribution Correlations

Conclusions made from reviewing the residual errors plots are as follows:

- Medium Tree and Bagged Trees regression models were the only models out of the 5 that produced flat profiles.
- Bagged Trees produced flat profiles for 100% of the 1 inch diameter by 2 inch high samples and 80% of the 2 inch diameter by 2 inch high samples.
- Just like the grayscale profiles, samples with a 0.75 inch diameter had a 0% chance of having an Annular distribution.
- Like the grayscale profiles, samples with a 0.75 inch height had a 20% chance of having an Annular distribution.
- Samples compressed to 125 and 150 thousandths had a higher chance (67%) of producing an Annular profile than samples compressed to 50, 75, or 100 thousandths (46%).

These correlations all come with logical explanations which are listed as follows:

- Due to Medium Tree and Bagged Tree models having similar regression structures, as well as each node within a data set for any sample used to create the modeling having the same compression depth values assigned these models are far more likely to create a Flat distribution across the surface. In addition, samples which have both height and diameter dimensions that the model has seen are more likely to be given equal compression depth values for each node.
- The low chance of an Annular distribution profile among 0.75 inch diameter and 0.75 inch high samples is caused by the same phenomenon that caused

it among the grayscale plots. Greater height variation across the printed surfaces led to larger prediction errors.

- The higher chance of an Annular distribution with a deeper compression depth is also caused by the same phenomenon that caused it among the grayscale plots. Greater compression depth creates a more uniform distribution across the contact surface.

4.4 Scatter Plots vs Contours

Contour plots were created to potentially display the scatter plot information in a more effective manner. To do this, Python was used to do the plotting since there was an open source add on that was designed for creating contour plots with scattered data, rather than using MATLAB and interpolating values to a meshgrid which accrued more error. An example of the contour output can be found below in Figure 4.10.

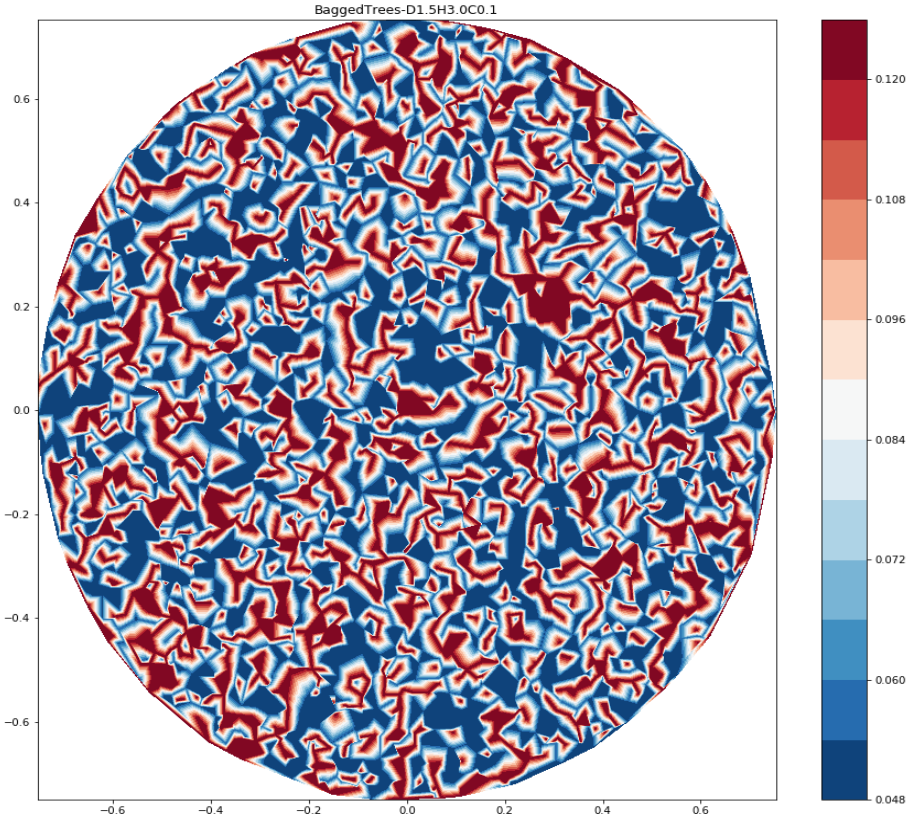

Figure 4.10: Contour Plot from Scatter Data

Although the contour plots displayed the information effectively, it did not attribute to a significant increase in clarity. However, when scatter plots were difficult to classify the contour plots were used as a second reference.

CHAPTER 5

CONCLUSIONS

5.1 Compression Depth Prediction Conclusions

For compression depth prediction, it has been concluded that there is no significant difference between an RMSE of a regression model trained with a 10% hold out value, 25% hold out value or a 3-fold cross-validation. Compression depth prediction results can be seen below in Table 5.1. The columns from left to right define the data set type being predicted, the best regression model to predict that data set, and the calculated RMSE of the predictions.

Table 5.1: Compression Depth Prediction Final Results

Data Set	Regression Model	RMSE
All Data	Linear	0.0230
Seen Diameters	Interactions Linear	0.0165
Seen Heights	Medium Tree	0.0172
Seen Heights & Diameters	Bagged Trees	0.001
Unseen Heights & Diameters	Linear SVM	0.0225

The goal of these predictions is to test the effectiveness of a regression model to predict how deep a cylindrical 3D printed cylinder had compressed given the geometry and grayscale values of its surface. The range of compression used for training the model was the same range used to test it. This ranged varied between 50 to 150 thousandths of an inch in increments of 25 thousandths. It can be concluded that this method can predict compression depths of samples with both seen heights and diameters well, being that the tests produced an RMSE of approximately one thousandth of an inch.

This methods ability to predict the compression depth of a sample with a height of diameter that is unseen to the trained model comes with significant error. A trained model better predicts a sample with an unseen height and seen diameter than it does a seen height and an unseen diameter, but not by much. In addition, giving the model inputs from samples with warped contact surfaces will lead to even more error in the predictions.

Ultimately, the compression depth can be predicted accurately for samples with geometry that it has seen before. For samples with at least one dimension unseen by the regression learner, compression depth can be predicted within 25 thousandths of an inch. The acceptability of this error is subject to its application.

5.2 Grayscale Value Prediction Conclusions

For grayscale value prediction, it has been concluded that there is no significant difference between an RMSE of a regression model trained with a 10% hold out value, 25% hold out value or a 3-fold cross-validation. Grayscale value prediction results can be found below in Table 5.2. The columns from left to right define the data set type being predicted, the best regression model to predict that data set, and the calculated RMSE of the predictions.

Table 5.2: Grayscale Value Prediction Final Results

Data Set	**Regression Model**	**RMSE**
All Data	Linear	0.293
Seen Diameters	Bagged Trees	0.2020
Seen Heights	Rational Quadratic GPR	0.2030
Seen Heights & Diameters	Bagged Trees	0.1370
Unseen Heights & Diameters	Quadratic SVM	0.2302

The goal of these predictions is to test the effectiveness of a regression model to predict the grayscale intensity, which can be converted to stress, of a sample given the geometry and compression depth. The range of grayscale values for all samples analyzed varied between 0.150 to 0.802. Due to the non-linearity of the grayscale-stress relationship, it is not possible to convert the RMSE directly from grayscale to stress.

Like predicting compression depth, predicting grayscale values across a sample face with diameters and heights that it has seen yields the lowest error. It can be said that any method to predict a grayscale value comes with a significant amount of error. This is likely due to the raster lines creating a variability of intensity across the top surface as well as warped surfaces on short samples. To conclude, the regression models built were unable to accurately predict grayscale values across any of the samples faces.

CHAPTER 6

FUTURE WORK

Future work for this research should be focused three main ideas: increasing data sets, studying vapor smoothing effects, applying concept to other geometries.

Increasing the data set sizes has on model accuracies would be beneficial to determining the best data set size for performing these studies. In addition, it would also test the repeatability of the research process. This could be accomplished by selecting more data points on existing surfaces, and/or adding the inputs from additional samples. The larger the input data set is for a ML regression model, the better that model will be at predicting the outputs. It is speculated that a second run of testing with a larger data set would attribute to better prediction accuracy.

Secondly, the samples could be vapor smoothed before being compressed. Vapor smoothing the contact surfaces would decrease the height variability of the outermost layers. This would make the contact surface less "jagged" while still capturing the behavior of the inner layers. In the end it would likely lead to more consistent grayscale values across the surface. An abstract example of how vapor smoothing would affect the outer layers of a printed sample can be seen below in Figure 6.1.

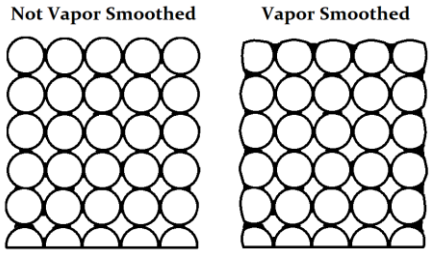

Figure 6.1: Vapor Smooth Comparison of 3D Printed Cylinders (Section View)

Lastly, studying the effectiveness of difference geometries would be beneficial to determine whether this method can be applied to non-circular geometries. Predicting the deformation and grayscale prediction of flat rectangular surfaces may be more accurate than predicting cylindrical surfaces due to the printing process. Slicing a rectangular surface may produce more consistent geometry in the samples. The printing head will only move in straight lines rather than between points that were fitted to a curve.

BIBLIOGRAPHY

3D Matter. (n.d.). *FDM 3D Printing materials compared*. Retrieved from 3D Hubs: https://www.3dhubs.com/knowledge-base/fdm-3d-printing-materials-compared/

3D Natives. (2018, December 6). *Additive manufacturing in aerospace is growing*. Retrieved from 3D Natives: https://www.3dnatives.com/en/additive-manufacturing-aerospace-growing-061220184/

3D Printing Industry. (2017). *The Free Beginner's Guide*. Retrieved from 3D Printing INdustry: https://3dprintingindustry.com/3d-printing-basics-free-beginners-guide#08-applications

3DSourced. (2018, July 4). *The Complete Guide to Lost Wax Casting and Wax 3D Printing*. Retrieved from 3DSourced: https://3dsourced.com/3d-printing-technologies/lost-wax-casting-3d-printing/

3DXTECH. (2020). *MAX-G™ GF-20 Glass Fiber Reinforced PETG [Discontinued]* . Retrieved from 3DXTECH Additive Manufacturing: https://www.3dxtech.com/max-g-gf-20-glass-fiber-reinforced-petg-discontinued/

ALT LLC. (n.d.). *Common 3D Printing Materials*. Retrieved from ALT LLC: https://www.3dalt.com/common-materials

ASTM D4673-16. (2016). *Standard Classification System for and Basis for Specification for Acrylonitrile–Butadiene–Styrene (ABS) Plastics and Alloys Molding and Extrusion Materials.* West Conshohocken, PA: ASTM International.

Bishop, C. M. (2006). *Pattern Recognition in Machine Learning.* Singapore: Springer.

Buddemeyer, D. (2018). Aligned with Growth. Eden Prairie, MN, United States of America.

Cantrell, J., Rhode, S., Damiani, D., Gurnani, R., DiSandro, L., Anton, J., . . . Ifju, P. (2016). Experimental Characterization of the Mechanical Properties of 3D Printed ABS and Polycarbonate Parts. *Advancement of Optical Methods in Experimental Mechanics, Volume 3*, 89-105.

Chowdhury, S., & Anand, S. (2016). Artificial neural network based geometric compensation for thermal deformation in additive manufacturing processes. *Proceedings of the 11th International Manufacturing Science and Engineering Conference.* Blacksburg.

Coleman, R. (2019, June 18). *Additive tech takes on short-run press brake tooling*. Retrieved from Canadian Fabricating and Welding: https://www.canadianmetalworking.com/canadianfabricatingandwelding/article/fabricating/additive-tech-takes-on-short-run-press-brake-tooling

Cortes, C., & Vapnik, V. (1995). Support-Vector Networks. *Machine Learning*, 273-297.

Crutchfield, B. (2018, May 3). *3D printing's impact on aerospace*. Retrieved from Aerospace Manufacturing and Design: https://www.aerospacemanufacturinganddesign.com/article/3d-printings-impact-on-aerospace/

Cyant. (2017, September 3). *Stereolithography Apparatus (SLA)*. Retrieved from Cyant: https://www.cyant.co/lexicon/2017/9/2/stereolithography-apparatus-sla

Dietterich, T. G. (2000). Ensemble Methods in Machine Learning. In MCS, *Lecture Notes in Computer Science* (Vol. 1857, pp. 1-15). Heidelberg, Berlin: Springer.

Disotell, K. (2018, August). Handbook for Technical Document Preparation. Youngstown, Ohio, United States.

Dokania, N. K., & Navneet, K. (2018). COMPARATIVE STUDY OF VARIOUS TECHNIQUES IN DATA MINING. *INTERNATIONAL JOURNAL OF ENGINEERING SCIENCES & RESEARCH TECHNOLOGY*, 202-209.

Durgun, I. (2015). Sheet metal forming using FDM rapid prototype tool. *Rapid Prototyping Journal*, 412-422.

Engineering Product Design. (n.d.). *Material Extrusion*. Retrieved from Engineering Product Design: https://engineeringproductdesign.com/knowledge-base/material-extrusion/

Engkvist, G. (2017). *Investigation of microstructure and mechanical properties of 3D printed Nylon.* Luleå University of Technology.

Estivill-Castro, V. (2002). Why so many clustering algorithms. *SIGKDD Explorations*, 65-75.

Fisher, R. A. (1936). The use of multiple measurements in taxonomic problems. *Annals of Eugenics*, 179-188.

Frick, L. (2014, April 29). *How to Smooth 3D-Printed Parts*. Retrieved from Machine Design: https://www.machinedesign.com/3d-printing/how-smooth-3d-printed-parts

Fujifilm. (n.d.). *Prescale*. Retrieved from Fujifilm Value from Innovation: https://www.fujifilm.com/products/prescale/prescalefilm/

Gandhi, R. (2018, May 27). *Introduction to Machine Learning Algorithms: Linear Regression*. Retrieved from Towards Data Science: https://towardsdatascience.com/introduction-to-machine-learning-algorithms-linear-regression-14c4e325882a

Gere, J. M., & Goodno, B. J. (2012). Mechanics of Materials. In J. M. Gere, & B. J. Goodno, *Mechanics of Materials* (p. 29). Stamford: Cengage Learning.

Gibson, I., Rosen, D. W., & Stucker, B. (2010). Additive Manufacturing Technologies. In I. Gibson, D. W. Rosen, & B. Stucker, *Rapid Prototyping to Direct Digital Manufacturing* (pp. 34-35). New York Heidelberg Dordrecht London: Springer.

Gregurić, L. (2019, February 11). *How Much Do 3D Printing Materials Cost in 2019?* Retrieved from ALL 3DP: https://all3dp.com/2/how-much-do-3d-printer-materials-cost/

Griffiths, L. (2018, September 11). The Magazine for Design-to-Manufacturing Innovation. *Align leverages 3D Systems' 3D printing to produce 320,000 custom aligners per day*. Rapid News Publications Ltd.

Hansen, L. K., & Salamon, P. (1990). Neural Network Ensembles. *IEEE Transactions on Pattern Analysis and Machine Intelligence*, 993-1001.

Hinton, G., & Sejnowski, T. J. (1999). *Unsupervised Learning: Foundations of Neural Computation.* Cambridge: The MIT Press.

Koza, J. R., Bennett, F. H., Andre, D., & Keane, M. A. (1996). AUTOMATED DESIGN OF BOTH THE TOPOLOGY AND SIZING OF ANALOG ELECTRICAL CIRCUITS USING GENETIC PROGRAMMING. In J. S. Gero, & F. Sudweeks, *Artificial Intelligence in Design* (pp. 151-170). Dordrecht: Springer.

Krogh, A., & Vedelsby, J. (1994). Neural Network Ensembles, Cross Validation, and Active Learning. *NIPS'94: Proceedings of the 7th International Conference on Neural Information Processing Systems*, (pp. 231-238).

Leacock, A., Volk, G., McCracken, D., & Brown, D. (2017). The use of Fused Deposition Modelled Tooling in Low Volume Production of Stretch Formed Double Curvature Components. *17th International Conference on Sheet Metal* (pp. 343-350). Newtownabbey: Procedia Engineering.

Loughborough University. (n.d.). *About Additive Manufacturing*. Retrieved from Additive Manufacturing Research Group: https://www.lboro.ac.uk/research/amrg/about/the7categoriesofadditivemanufacturing/

McCue, T. (2019, November 14). *STL Files: What They Are and How to Use Them*. Retrieved from Lifewire: https://www.lifewire.com/stl-files-2255

Miller, A. (2016, August 1). *The Evolution of 3D Printing: Past, Present and Future*. Retrieved from 3D Printing Industry: https://3dprintingindustry.com/news/evolution-3d-printing-past-present-future-90605/

Nikam, S. S. (2015). A Comparative Study of Classification Techniques in Data Mining Algorithms. *ORIENTAL JOURNAL OF COMPUTER SCIENCE & TECHNOLOGY*, 13-19.

Otsu, N. (1979). A Threshold Selection Method from Gray-Level Histograms. *IEEE Transactions on Systems, Man, and Cybernetics, 9*(1), 62-66. doi:10.1117/1.1631315

Palermo, E. (2013, September 19). *Fused Deposition Modeling: Most Common 3D Printing Method*. Retrieved from Live Science: https://www.livescience.com/39810-fused-deposition-modeling.html

Panda, B. N., Bahubalendruni, R., & Biswal, B. B. (2015). A general regression neural network approach for the evaluation of compressive strength of FDM prototypes. *Neural Computing and Applications*, 1129-1136.

Perrone, M. P., & Cooper, L. N. (1992). *When Networks Disagree: Ensemble Methods for Hybrid Neural Networks.* Providence: BROWN UNIV PROVIDENCE RI INST FOR BRAIN AND NEURAL SYSTEMS.

Prod Ways Tech. (n.d.). *Lost Wax Casting Patterns*. Retrieved from Prod Ways Tech: https://www.prodways.com/en/industrial_segment/dental/lost-wax-patterns-rpd-bridges-crowns/

Prototype Projects. (2018). *FDM - Fused Deposition Modelling.* Retrieved from Prototype Projects: https://www.prototypeprojects.com/technologies/fdm-prototyping/

Rainbow Aviation Services. (2018, January 11). *3D Printed Press Brake Dies for Building The EMG-6* . Retrieved from Rainbow Aviation Services: https://electricmotorglider.com/2018/01/11/press_brake_dies/

Rasmussen, C. E., & Williams, K. I. (2006). *sian Processes for Machine Learning, the MI.* Cambridge: The MIT Press.

Ray, S. (2017, September 13). *Understanding Support Vector Machine algorithm from examples (along with code)*. Retrieved from Analytics Vidhya: https://www.analyticsvidhya.com/blog/2017/09/understaing-support-vector-machine-example-code/

Reid, S. (2007, February 15). A Review of Heterogeneous Ensemble Methods. Boulder, Colorado, USA: University of Colorado at Boulder: Department of Computer Science.

Reimann, D., Nidadavolu, K., Hassan, H. u., Vajragupta, N., Glasmachers, T., Junker, P., & Hartmaier, A. (2019). Modeling Macroscopic Material Behavior With Machine Learning Algorithms Trained by Micromechanical Simulations. *Frontiers in Materials*.

Russell, S. J., & Norvig, P. (2010). *Artificial Intelligence: A Modern Approach, Third Addition.* Englewood Cliffs: Prentice Hall.

Samuel, A. L. (1959). Some studies in machine learning using hte game of Checkers. *IBM Journal of Research and Development*, 71-105.

Sano, K., Ishida, Y., & Aida, T. (2017). Synthesis of Anisotropic Hydrogels and Their Applications. *Angewandte Chemie International Edition*, 2532-2535.

Star Rapid. (2016, April 3). *What Is G-Code And Why Is It Important For Your Parts?* Retrieved from Star Rapid: https://www.starrapid.com/blog/what-is-g-code-and-why-is-it-important-for-your-parts/

The MathWorks, Inc. (2019). *Choose Regression Model Options*. Retrieved from MathWorks: https://www.mathworks.com/help/stats/choose-regression-model-options.html#bvmnwhd-1

The MathWorks, Inc. (2019). *Decision Trees*. Retrieved from MathWorks: https://www.mathworks.com/help/stats/decision-trees.html?s_tid=srchtitle

The MathWorks, Inc. (2019). *Kernel (Covariance) Function Options*. Retrieved from MathWorks: https://www.mathworks.com/help/stats/kernel-covariance-function-options.html

Tukey, J. (1961). *The Future of Data Analysis.*

Turner, D. R. (2016). *Gaussian Processes: From the Basics to the State-of-the-Art.* Retrieved from http://cbl.eng.cam.ac.uk/pub/Public/Turner/News/imperial-gp-tutorial.pdf

Ulintz, P. (2015, December 1). *Tooling by Design.* Retrieved from Metal Forming Magazine: https://www.metalformingmagazine.com/magazine/article/?/2015/12/1/A_Brief_History_of_the_Tool_and_Die_Industry

Vapnik, V. N. (1982). *Estimation o fDependences Based on Empirical Data.* New York: Springer.

Wang, J., Neskovic, P., & Cooper, L. N. (2005). Training Data Selection for Support Vector Machines. *Lecture Notes in Computer Science*, (pp. 554-564).

Weisberg, S. (2005). Applied Linear Regression. In S. Weisberg, *Applied Linear Regression* (p. 21). Hoboken: John Wiley & Sons, Inc.

Wu, H., Wang, Y., & Yu, Z. (2016). In situ monitoring of FDM machine condition via acoustic emission. *The International Journal of Advanced Manufacturing Technology*, 1483-1495.

Zhang, Y., Hong, G. S., Ye, D., Zhu, K., & Fuh, J. Y. (2018). Extraction and evaluation of melt pool, plume and spatter information for powder-bed fusion AM process monitoring. *Materials & Design*, 458-469.

Zhao, Z., & Liu, H. (2007). Spectral Feature Selection for Supervised and Unsupervised Learning. In *ACM International Conference Proceeding Series* (pp. 1151-1157). doi:10.1145/1273496.1273641

Ziemian, C., Sharma, M., & Ziemian, S. (2012). Anisotropic Mechanical Properties of ABS Parts Fabricated by Fused Deposition Modelling. In M. Gokcek, *Mechanical Engineering* (pp. 159-180). Rijeka: InTech.

Zou, R. &.-b. (2016). Isotropic and anisotropic elasticity and yielding of 3D printed material. *Composites Part B: Engineering*, 506-513.

APPENDICIES

Appendix A:Printing Parameters

QUALITY	100% INFILL DENSITY SETTINGS	SPEED	
Layer Height	0.22	Print Speed	60
Initial Layer height	0.3	Infill Speed	60
Line Width	0.5	Wall Speed	30
Wall Line Width	0.5	Outer Wall Speed	30
Outer Wall Line Width	0.5	Inner Wall Speed	60
Inner Wall Line Width	0.5	Top/Bottom Speed	30
Top/Bottom Line Width	0.5	Travel Speed	120
Infill Line Width	0.5	Initial Layer Speed	30
Skirt/Brim Line Width	0.5	Initial Layer Print Speed	30
SHELL		Initial Layer Travel Speed	60
Wall Thickness	0.8	Skirt/Brim Speed	30
Wall Line Count	2	Maximum Z Speed	0
Outer Wall Wipe Distance	0.25	Number of Slower Layers	4
Top/Bottom Thickness	0.8	Equalize Filament Flow	Off
Top Thickness	0.8	Enable Acceleration Control	Off
Top Layers	0	Enable Jerk Control	On
Bottom Thickness	0.8	Print Jerk	12
Bottom Layers	999999	Infill Jerk	12
Top/Bottom Pattern	Lines	Wall Jerk	12
Bottom Pattern Initial Layer	Lines	Outer Wall Jerk	12
Top/Bottom Line Directions	[]	Inner Wall Jerk	12
Outer Wall Inset	0	Top/Bottom Jerk	12
Outer Before Inner Walls	Off	Travel Jerk	12
Alternate Extra Wall	On	Initial Layer Jerk	12
Compensate Wall Overlaps	On	Initial Layer Print Jerk	12
Compensate Inner Wall Overlaps	On	Initial Layer Travel Jerk	12
Fill Gaps Between Walls	On	Skirt/Brim Jerk	12
Horizontal Expansion	Everywhere	**TRAVEL**	
Z Seam Alignment	0	Combing Mode	All
Ignore Small Z Gaps	On	Retract Before Outer Wall	Off
Extra Skin Wall Count	1	Avoid Printed Parts When Traveling	On
Enable Ironing	Off	Travel Avoidance Distance	0.625
INFILL		Layer Start X	100
Infill Density	100%	Layer Start Y	100

Infill Line Distance	0.5
Infill Pattern	Lines
Infill Line Directions	[]
Infill Overlap Percentage	0
Infill Overlap	0
Skin Overlap Percentage	5
Skin Overlap	0.025
Infill Wipe Distance	0.125
Infill Layer Thickness	0.22
Gradual Infill Steps	0
Infill Before Walls	Off
Minimum Infill Area	0
Skin Expand Distance	1
Maximum Skin Angle for Expansion	90
Minimum Skin Width for Expansion	0
MATERIAL	
Default Printing Temperature	245
Printing Temperature	245
Probe Temperature	160
Soften Temperature	170
Wipe Temperature	160
Printing Temperature Initial Layer	250
Initial Printing Temperature	235
Final Printing Temperature	230
Extrusion Cool Down Speed Modifier	0.7
Build Plate Temperature	72.5
Part Removal Temperature	17.5
Keep Heating	On
Build Plate Temperature Initial Layer	100
Diameter	2.85
Flow	96
Initial Layer Flow Rate	100
Enable Retraction	Off
Retract at Layer Change	Off
Standby Temperature	0

COOLING	
Enable Print Cooling	Off
Regular/Maximum Fan Speed Threshold	10
Regular Fan Speed at Height	0.3
Regular Fan Speed at Layer	2
Minimum Layer Time	5
Minimum Speed	10
Lift Head	Off
SUPPORT	
Generate Support	Off
BUILD PLATE ADHESION	
Build Plate Adhesion Type	None
Build Plate Adhesion Extruder	
Skirt/Brim Minimum Length	
Brim Width	
Brim Line Count	
Brim Only on Outside	
DUAL EXTRUSION	
Enable Prime Tower	Off
Enable Ooze Shield	Off
MESH FIXES	
Union Overlapping Volumes	On
Remove All Holes	Off
Extensive Stitching	Off
Keep Disconnected Faces	Off
Merged Meshes Overlap	0.15
Remove Mesh Intersection	On
Alternate Mesh Removal	On
SPECIAL MODES	
Mold	Off
Surface Mode	Normal
Spiral Outer Contour	Off
EXPERIMENTAL	
Enable Draft Shield	Off
Make Overhang Printable	Off
Enable Coasting	Off
Alternate Skin Rotation	Off
Spaghetti Infill	Off
Fuzzy Skim	Off
Wire Printing	Off

Appendix B:Grayscale Value Training Data RMSE

The training data RMSE values for grayscale regression models can be found below. The minimum of each row is outlined with a bold box.

3-fold Cross-Validation	0.19462	0.1851	0.19702	0.18974	0.16172	0.1542	0.15598	0.20198	0.20069	0.18384	0.16311	0.17656	0.19693	0.18381	**0.14166**	0.16488	0.16055	0.15433	0.15731
10% Holdout	0.19035	0.18559	0.19223	0.18571	0.15347	0.14698	0.14961	0.19718	0.19503	0.1778	0.15824	0.17003	0.19176	0.16927	**0.13514**	0.16052	0.15407	0.14938	0.15036
25% Holdout	0.1934	0.18887	0.19566	0.18913	0.16139	0.15298	0.15383	0.20061	0.19945	0.18308	0.16254	0.17517	0.19589	0.17261	**0.14025**	0.16407	0.15952	0.15286	0.16063
StdDev (Population)	0.00216	0.00232	0.00243	0.00242	0.0056	0.00424	0.00298	0.00243	0.00313	0.00373	0.00304	0.00363	0.00292	0.00236	0.00361	0.00251	0.00385	0.00246	0.00726

Appendix C: Grayscale Value Testing Data RMSE

The testing data RMSE values for grayscale regression models and all validation types can be found below. The minimum of each row is outlined with a bold box.

	RMSE for model testing results	Linear	Interactions Linear	Robust Linear	Stepwise Linear	FineTree	Medium Tree	Coarse Tree	LinearSVM	Quadratic SVM	Cubic SVM	FineGaussian SVM	Medium Gaussian SVM	Coarse Gaussian SVM	Boosted Trees	Bagged Trees	Squared Exponential GPR	Matern 5_2 GPR	Exponential GPR	Rational Quadratic GPR
3-fold Cross Validation (3fcv)	**ALL DATA**	**0.2393**	**0.8179**	**0.2438**	**1.1028**	**0.2835**	**0.2750**	**0.2692**	**0.2452**	**0.2609**	**0.4736**	**0.2444**	**0.2786**	**0.2513**	**0.2586**	**0.2537**	**0.2465**	**0.2623**	**0.2692**	**0.2801**
	ONLY SEEN DIAMETERS	0.2130	0.2109	0.2149	0.2099	0.2137	0.2091	0.2104	0.2178	0.2168	0.2410	0.2062	0.2247	0.2170	0.2160	0.2018	0.2081	0.2142	0.2185	0.2304
	ONLY SEEN HEIGHTS	0.2426	0.7379	0.2493	1.0096	0.2690	0.2604	0.2526	0.2504	0.2797	0.3217	0.2218	0.2288	0.2375	0.2441	0.2322	0.2152	0.2126	0.2033	0.2047
	SEEN DIAMETER AND HEIGH	0.1961	0.1913	0.1989	0.1915	0.1524	0.1481	0.1513	0.2046	0.2035	0.1864	0.1612	0.1782	0.1991	0.1752	0.1367	0.1654	0.1602	0.1530	0.1549
	UNSEEN HEIGHT AND DIAM	0.2341	1.1573	0.2367	1.5516	0.3114	0.3012	0.2951	0.2401	0.2364	0.7480	0.2753	0.3581	0.2828	0.2810	0.2810	0.2922	0.3339	0.3572	0.3743
10% Hold Out Validation (10hoval)	**ALL DATA**	**0.2393**	**0.8179**	**0.2438**	**1.1028**	**0.2835**	**0.2750**	**0.2692**	**0.2450**	**0.2744**	**0.3863**	**0.2444**	**0.2786**	**0.2513**	**0.2586**	**0.2526**	**0.2432**	**0.2603**	**0.2699**	**0.2690**
	ONLY SEEN DIAMETERS	0.2130	0.2109	0.2149	0.2099	0.2137	0.2091	0.2104	0.2173	0.2163	0.2348	0.2062	0.2247	0.2170	0.2160	0.2020	0.2056	0.2138	0.2190	0.2245
	ONLY SEEN HEIGHTS	0.2426	0.7379	0.2493	1.0096	0.2690	0.2604	0.2526	0.2504	0.3049	0.2692	0.2218	0.2288	0.2375	0.2441	0.2293	0.2155	0.2124	0.2034	0.2030
	SEEN DIAMETER AND HEIGH	0.1961	0.1913	0.1989	0.1915	0.1524	0.1481	0.1513	0.2040	0.2034	0.1865	0.1612	0.1782	0.1991	0.1752	0.1370	0.1646	0.1605	0.1528	0.1535
	UNSEEN HEIGHT AND DIAME	0.2341	1.1573	0.2367	1.5516	0.3114	0.3012	0.2951	0.2396	0.2302	0.5904	0.2753	0.3581	0.2828	0.2810	0.2818	0.2843	0.3290	0.3584	0.3507
25% Hold Out Validation (25hoval)	**ALL DATA**	**0.2393**	**0.8179**	**0.2438**	**1.1028**	**0.2835**	**0.2750**	**0.2692**	**0.2451**	**0.2671**	**0.5120**	**0.2444**	**0.2786**	**0.2513**	**0.2586**	**0.2549**	**0.2437**	**0.2559**	**0.2702**	**0.2874**
	ONLY SEEN DIAMETERS	0.2130	0.2109	0.2149	0.2099	0.2137	0.2091	0.2104	0.2177	0.2169	0.2477	0.2062	0.2247	0.2170	0.2160	0.2037	0.2053	0.2132	0.2191	0.2332
	ONLY SEEN HEIGHTS	0.2426	0.7379	0.2493	1.0096	0.2690	0.2604	0.2526	0.2503	0.2925	0.3499	0.2218	0.2288	0.2375	0.2441	0.2320	0.2156	0.2153	0.2034	0.2059
	SEEN DIAMETER AND HEIGH	0.1961	0.1913	0.1989	0.1915	0.1524	0.1481	0.1513	0.2045	0.2038	0.1861	0.1612	0.1782	0.1991	0.1752	0.1371	0.1654	0.1585	0.1527	0.1565
	UNSEEN HEIGHT AND DIAME	0.2341	1.1573	0.2367	1.5516	0.3114	0.3012	0.2951	0.2400	0.2306	0.8098	0.2753	0.3581	0.2828	0.2810	0.2829	0.2866	0.3116	0.3590	0.3908

Appendix D: Compression Depth Training Data RMSE

The training data RMSE values for compression depth regression models can be found below. The minimum of each row is outlined with a bold box.

3-fold Cross-Validation	0.02	0.0174	0.0204	0.0177	0.0013	0.0014	0.002	0.0206	0.0187	0.0113	0.0131	0.0137	0.0215	0.0109	0.001	0.0097	0.0155	0.0095	0.0101
10% Holdout	0.0202	0.0176	0.0207	0.0179	0.0013	0.0014	0.0019	0.021	0.0193	0.0122	0.0138	0.0143	0.0222	0.011	0.001	0.0098	0.0189	0.0097	0.0093
25% Holdout	0.0203	0.0177	0.0208	0.018	0.0016	0.0016	0.0022	0.0212	0.0193	0.0119	0.0139	0.0146	0.0224	0.0107	0.0011	0.0098	0.0183	0.0102	0.0106
StdDev (Population)	0.0002	0.0001	0.0002	0.0001	0.0002	0.0001	0.0002	0.0003	0.0004	0.0005	0.0004	0.0005	0.0005	0.0002	2E-05	5E-05	0.0018	0.0004	0.0006

Appendix E: Compression Depth Testing Data RMSE

	RMSE for model testing results	Linear	Interactionslinear	Robust Linear	Stepwise Linear	Fine Tree	Medium Tree	Coarse Tree	Linear SVM	Quadratic SVM	Cubic SVM	Fine Gaussian SVM	Medium Gaussian SVM	Coarse Gaussian SVM	Boosted Trees	Bagged Trees	Squared Exponential GPR	Matern 5_2GPR	Exponential GPR	Rational Quadratic GPR
3-fold Cross Validation (3fcv)	**ALL DATA**	**0.0010**	**0.3951**	**0.0254**	**0.2876**	**0.0321**	**0.0321**	**0.0321**	**0.0250**	**0.1324**	**0.2955**	**0.0240**	**0.1035**	**0.0318**	**0.0249**	**0.0360**	**0.7531**	**0.0271**	**0.1141**	**0.9455**
	ONLY SEEN DIAMETERS	0.0188	0.0165	0.0207	0.0183	0.0220	0.0220	0.0221	0.0211	0.0207	0.2051	0.0173	0.0554	0.0258	0.0203	0.0220	0.1595	0.0178	0.0446	0.1748
	ONLY SEEN HEIGHTS	0.0249	0.3768	0.0274	0.2750	0.0172	0.0172	0.0172	0.0275	0.1253	0.1764	0.0214	0.1109	0.0247	0.0173	0.0186	0.4689	0.0288	0.1001	0.7177
	SEEN DIAMETER AND HI	0.0205	0.0179	0.0211	0.0182	0.0017	0.0017	0.0020	0.0214	0.0192	0.0119	0.0133	0.0142	0.0224	0.0110	0.0010	0.0095	0.0192	0.0094	0.0095
	UNSEEN HEIGHT AND D	0.0233	0.5395	0.0242	0.3915	0.0490	0.0490	0.0490	0.0225	0.1812	0.4349	0.0296	0.0985	0.0436	0.0334	0.0574	1.2719	0.0297	0.1569	1.4907
10% Hold Out Validation (10hoval)	**ALL DATA**	**0.0230**	**0.3951**	**0.0254**	**0.2876**	**0.0321**	**0.0321**	**0.0321**	**0.0251**	**0.1232**	**0.3838**	**0.0240**	**0.1035**	**0.0318**	**0.0249**	**0.0360**	**0.2926**	**0.0277**	**0.1271**	**0.5062**
	ONLY SEEN DIAMETERS	0.0188	0.0165	0.0207	0.0183	0.0220	0.0220	0.0221	0.0211	0.0201	0.2789	0.0173	0.0554	0.0258	0.0203	0.0220	0.0891	0.0177	0.0527	0.1285
	ONLY SEEN HEIGHTS	0.0249	0.3768	0.0274	0.2750	0.0172	0.0172	0.0172	0.0275	0.1174	0.2001	0.0214	0.1109	0.0247	0.0173	0.0185	0.0836	0.0279	0.1102	0.1788
	SEEN DIAMETER AND HI	0.0205	0.0179	0.0211	0.0182	0.0017	0.0017	0.0020	0.0213	0.0193	0.0115	0.0133	0.0142	0.0224	0.0110	0.0010	0.0112	0.0190	0.0092	0.0104
	UNSEEN HEIGHT AND D	0.0233	0.5395	0.0242	0.3915	0.0490	0.0490	0.0490	0.0226	0.1674	0.5767	0.0296	0.0985	0.0436	0.0334	0.0574	0.5391	0.0330	0.1751	0.9273
25% Hold Out Validation (25hoval)	**ALL DATA**	**0.0230**	**0.3951**	**0.0254**	**0.2876**	**0.0321**	**0.0321**	**0.0321**	**0.0250**	**0.1324**	**0.3383**	**0.0240**	**0.1035**	**0.0318**	**0.0249**	**0.0361**	**0.7276**	**0.1263**	**0.1019**	**1.0749**
	ONLY SEEN DIAMETERS	0.0188	0.0165	0.0207	0.0183	0.0220	0.0220	0.0221	0.0211	0.0207	0.2402	0.0173	0.0554	0.0258	0.0203	0.0220	0.1554	0.0541	0.0387	0.1895
	ONLY SEEN HEIGHTS	0.0249	0.3768	0.0274	0.2750	0.0172	0.0172	0.0172	0.0275	0.1253	0.1873	0.0214	0.1109	0.0247	0.0173	0.0187	0.4531	0.1039	0.0908	0.8535
	SEEN DIAMETER AND HI	0.0205	0.0179	0.0211	0.0182	0.0017	0.0017	0.0020	0.0214	0.0192	0.0117	0.0133	0.0142	0.0224	0.0110	0.0011	0.0097	0.0143	0.0097	0.0093
	UNSEEN HEIGHT AND D	0.0233	0.5395	0.0242	0.3915	0.0490	0.0490	0.0490	0.0225	0.1812	0.5052	0.0296	0.0985	0.0436	0.0334	0.0574	1.2285	0.1803	0.1389	1.6584